

**POLYTECHNIC OF TURIN
UNIVERSITY OF SOUTHAMPTON**

Master's Degree in Aerospace Engineering



Master's Degree Thesis

**Optimization of a Hydrofoiling
International Moth design and
performance investigations with a 6 DOF
dynamic model**

Supervisors

Prof. Giuliana MATTIAZZO

Prof. Stephen R.TURNOCK

Candidate

Salvatore BUCARIA

A.Y. 2021/2022

Abstract

Hydrofoiling boats represent the cutting-edge of the world of sailing. Their ability of “flying over the water” makes them one of the most fascinating challenges for designers. The increasing complexity results in the need to find trade-offs across the multiple specialist areas involved, in order to achieve a successful project. Hence the importance in the development of design tools capable of “foreseeing the future”. This thesis work aims to contribute to all design stages, from the preliminary to the more detailed, of an *International Moth*. At first, the high-level requirements are identified, imposed by the sailor’s needs, manufacturing’s limits and performance. Therefore, an **optimization tool** is implemented, by exploiting global and local optimization algorithms, aiming to determine the best boat’s configuration capable to be compliant with requirements. Considerable emphasis is placed on the stability concepts, by analysis both static and dynamic aspects through the small perturbation theories.

The need to move a step towards the reality and to simulate the performance of the resulting design, leads to the development of a **6 DOF dynamic model**. The model allows for sailor-boat interactions and stability assessments, as well as manoeuvres simulations. Sailor’s movements and adjustments are reproduced by means of controllers on sail, rudder and rudder-foil. An in-depth study of the main foil control system is provided, highlighting its performance and its crucial role in ensuring a stable flight.

Acknowledgements

I would like to express my gratitude to my supervisor professor Giuliana Mattiazzo, for giving me the opportunity to better express my ideas and skills. Thanks to professors Stephen Turnock and Stephen Boyd for bringing me through one of the most enriching experiences of my life and for getting me further passionate about the world of sailing.

A great thanksgiving goes to Pietro Casalone and Oronzo Dell'Edera for supporting and believing in me from the first to the last moment of this work.

Finally, I dedicate this work to all those people who have been with me during this university journey. You know how difficult it was, but together we succeeded.

Table of Contents

List of Tables	VI
List of Figures	VII
Acronyms	X
1 Introduction	1
1.1 Motivation	1
1.2 State of Art	2
1.3 International Moth Class	2
1.4 Thesis structure description	4
2 Sailing Background	5
2.1 True and Apparent Wind	5
2.2 Physic behind	7
2.3 Main foil control system	7
3 Optimization Tool	11
3.1 Methodology	14
3.2 Static Model	15
3.3 Static Stability Evaluation	19
3.4 Dynamic Stability: linearized model	19
3.4.1 Small perturbation theory	20
3.4.2 Longitudinal stability	22
3.4.3 Derivatives	23
3.5 Results	29
4 6 DOF dynamic model	33
4.1 Motivation and assumptions	33
4.2 Reference systems and model variables	34
4.3 Force modules	37

4.3.1	Foils	37
4.3.2	Vertical appendages	39
4.3.3	Hull	40
4.3.4	Sail	41
4.4	Equilibrium equations	41
4.5	Controllers	44
4.5.1	Main foil control system	44
4.5.2	Rudder foil control system	45
4.5.3	Rudder directional control system	46
4.5.4	Roll motion control	46
4.6	Simulation results	49
5	Stability assessments	54
6	Maneuvers	59
7	Conclusion and future work	63
A	Appendix	65
A.1	Forces components	65
A.2	Inertia of the system	67
A.3	Control systems	68
A.3.1	Mach2	68
A.3.2	BugsCam	70
A.4	Fixed data	73
	Bibliography	75

List of Tables

3.1	Boundaries on design variables	15
3.2	Boundaries on state variables	18
3.3	Parameters of modal response	21
3.4	Results: Design variables	30
3.5	Results: main and rudder foil's geometry	31
3.6	Results: modes	32
3.7	Results: decay time	32
4.1	State variables	36
4.2	Regression parameters	49
5.1	Dynamic response characteristics	56
5.2	Impulsive disturbance	57
A.1	fixed model data	74

List of Figures

1.1	International Moth	3
2.1	True and Apparent wind [3]	6
2.2	Sailing Courses [8]	6
2.3	Sail Forces direction [3]	8
2.4	Transmission line [5]	9
2.5	Mach 2	10
2.6	Bugs Cam	10
3.1	Sailor-boat interactions [4]	12
3.2	Algorithm flow chart	16
3.3	Reference frames 2 DOF model	17
3.4	$C_{M\alpha}$ linear approximation	20
3.5	Root Loci [14]	22
3.6	Reference frame and state variables	23
3.7	Derivatives contributions	25
3.8	Vertical speed effect	26
3.9	Pitch rate effect	28
3.10	Results: GA iterations - equilibrium solutions	31
3.11	Results: static stability	31
3.12	Results: eigenvalues - stability diagram	32
4.1	Reference frames 6 DOF: top,lateral,rear views	35
4.2	DOF names	37
4.3	Main and rudder foil aerodynamic angles	38
4.4	Sail polars	41
4.5	Mach2: performance curve	45
4.6	BugsCam: performance curve	45
4.7	Roll motion control	47
4.8	Results: TWS = 5 m/s TWA = 50°: AWA variation	50
4.9	Results TWS = 5 m/s TWA = 50°: speeds,body forces	50

4.10	Results TWS = 5 m/s TWA = 50°: TO speed, control system . . .	51
4.11	Results TWS = 5 m/s TWA = 50°: longitudinal,roll motion,directional controls	52
4.12	Results: TWS = 8 m/s TWA = 50°: AWA variation	52
4.13	Results TWS = 8 m/s TWA = 50°: TO, flap, longitudinal, roll motion	53
5.1	TWS = 8 m/s TWA = 50° : Eigenvalues	55
5.2	Linear and Non-linear response ($\Delta h = 0.15m$)	55
5.3	Flap effect: Eigenval	56
5.4	Flap effect: time response	57
5.5	Response to impulsive disturbance $\Delta h = 0.15m$	58
5.6	Response to sinusoidal disturbance	58
6.1	Bearing Away maneuver [21]	59
6.2	Maneuver: AWA variation, BugsCam control system	60
6.3	Maneuver: X,Y,Z body forces	61
6.4	Maneuver: Longitudinal, Roll motion control	61
6.5	Maneuver: 3D path	62
A.1	Mach2: real system	69
A.2	Mach2: model variables	69
A.3	Mach2: sensitivity	70
A.4	Mach2: model	70
A.5	Mach2: performance	71
A.6	BugsCam: curve	72
A.7	BugsCam: sensitivity	72
A.8	BugsCam: performance	73

Acronyms

AoA Angle of Attack

AR Aspect Ratio

AWA Apparent Wind Angle

AWS Apparent Wind Speed

CoG Centre of gravity

DOF Degree of freedom

DVPP Dynamic Velocity Prediction Program

TWA True Wind Angle

TWS True Wind Speed

VPP Velocity Prediction Program

Nomenclature

α	Aerodynamic angle of attack
α_0	Zero lift angle of attack
α_g	Geometric angle of attack
α_{flap}	Flap deflection
α_{wand}	Sensor wand angle
\bar{c}	Mean Aerodynamic Chord
$\tau = \frac{\delta\alpha}{\delta\alpha_{flap}}$	Effect of flap angle on the angle of attack
$\vec{\omega}$	Angular speed vector around body axes
$\vec{i}, \vec{j}, \vec{k}$	Unit vectors
\vec{K}	Angular momentum
\vec{Q}	Momentum
\vec{u}	Command vector
\vec{V}_i	right eigenvectors
\vec{W}_i	left eigenvectors
\vec{x}_0	Initial state vector
\vec{x}	State vector
\vec{y}	Output vector
$a = C_{L\alpha 2D}$	2D lift curve slope
A	State matrix

a, b Real and imaginary part of eigenvalues
 $a_{3D} = C_{L_{\alpha 3D}}$ 3D lift curve slope
 B Command matrix
 c Chord
 C_D Drag coefficient
 C_L Lift coefficient
 C_M Pitching moment coefficient
 $C_{D\alpha} = \frac{\delta C_D}{\delta \alpha}$ Derivative of drag coefficient w.r. angle of attack
 $C_{Dh} = \frac{\delta C_D}{\delta h}$ Derivative of drag coefficient w.r. submerged length
 C_{D0} Shape drag
 C_{Di} Induced drag
 $C_{D_{wv}}$ Wave drag coefficient
 $C_{L\alpha} = \frac{\delta C_L}{\delta \alpha}$ Derivative of lift coefficient w.r. angle of attack
 $C_{Lh} = \frac{\delta C_L}{\delta h}$ Derivative of lift coefficient w.r. submerged length
 $C_{L\infty}$ Lift coefficient without free surface effect
 C_{M0} Zero Pitching moment coefficient
 $C_{M\alpha}$ Derivative of pitching moment coefficient
 c_{root} Root Chord
 c_{tip} Tip Chord
 e Oswald factor
 $F_x, F_y, F_z, M_x, M_y, M_z$ Body forces and moments
 h Submerged length
 i Setting angle
 $K_0 = \frac{g}{v^2}$ Correction factor on wave drag effect
 K_1, K_2 Weighted factors of the objective function

K_{mf}, K_{rf} Inertia factors
 L_D, L_R Daggerboard and Rudder length
 l_D, l_R Daggerboard and Rudder submerged length
 l_{wand} Wand's length
 $l_{x_{mf}} = x_g - x_{mf}$ Longitudinal distance of main foil w.r CoG
 $l_{x_{rf}} = x_{rf} - x_g$ Longitudinal distance of rudder foil w.r CoG
 $l_{z_{mf}} = z_g + z_{mf}$ Vertical distance of main foil w.r CoG
 $l_{z_{rf}} = z_g + z_{rf}$ Vertical distance of rudder foil w.r CoG
 M_{ctr} Roll motion control factor
 p Sail power factor
 P_1, P_2, P_3 Interpolating factors of main foil control system law
 V Boat's Speed
 x_b, y_b, z_b Body axes
 x_g, y_g, z_g Coordinates of CoG
 x_I, y_I, z_I Inertial axes
 $x_D = x_{mf}$ Longitudinal distance of daggerboard's centre of effort w.r to the bow
 x_{mf} Longitudinal distance of main foil's centre of effort w.r to the bow
 x_{rf} Longitudinal distance of rudder foil's centre of effort w.r to the bow
 $x_R = x_{rf}$ Longitudinal distance of rudder's centre of effort w.r to the bow
 z_D Vertical distance of daggerboard's centre of effort w.r to the CoG
 z_{mf} Vertical distance of main foil's centre of effort w.r to the deck plane
 z_{rf} Vertical distance of rudder foil's centre of effort w.r to the deck plane
 z_R Vertical distance of rudder's centre of effort w.r to the CoG
 D Subscript for "daggerboard"
 mf Subscript for "main foil"
 rf Subscript for "rudder foil"
 R Subscript for "rudder"

Chapter 1

Introduction

1.1 Motivation

The reasons behind this work stem from two challenges I have faced during my experience as a member of the “dynamic and performance section” at *PoliTo sailing team*¹, when I have been involved into the project of our first International Moth. The first challenge concerns the need to fill the gap between the preliminary design stages and the final product. In fact, one of the keys for the project’s successes rely on having a vision as clear as possible of the final purposes, starting from the very early stages. Despite this "prediction work" involves thousands of unknowns and some assumptions must be made to go on, it allows the following design phases to be constantly in line with the main basic concept. Consequently, the development of a design **optimization tool** aiming to define the preliminary boat’s configuration according to pre-established requirements.

Secondly, if the strength of a project is proved by how forward-looking the preliminary designers are, it is also true that, as the project progresses, there is a constant need to look back, verify the impact of the current decisions on the final product and try to find a compromise among the different project’s needs. Hence, the development of a **6 DOF dynamic model** with the goal to investigate boat’s performance, stability and sailor-boat interaction.

Therefore, this thesis is divided into two parts: firstly, the priority is given on finding the optimum *Moth*’s design and secondly, its dynamic behavior is deeply analysed.

¹<https://areweb.polito.it/politosailingteam/index.php>

1.2 State of art

The state of art of foiling boats' preliminary design tools is represented by a large number of softwares able to evaluate both static and dynamic performance.

One of the most renowned is *FS-equilibrium*[1] (Future Ship), an open modular workbench created by the Fluid Engineering Department of the classification society and maritime advisor *DNV GL*. It is a modular and a multi-purpose tool which is suitable for different sailboat classes. Users, after entering the geometric, hydrodynamic and inertial proprieties, are asked to select among different pre-defined force modules in order to build the mathematical model. However, importing data from external sources, such as CFD analysis results, is an option too. Finally, boat's performance and maneuvers are simulated with high-fidelity results.

Another tool worthy of mention is *Typhoon* [2], developed by the *University of Ghent*. With a user-friendly interface, capable of reproducing the desired foil's configuration, this software calculates the equilibrium point, the trim conditions and investigate the dynamic response to a small disturbance by using the "Vortex-lattice method" to evaluate forces.

Moreover, one of the most innovative approach into the foiling boats' design is given by Rafael Tannenbergs [3]. The goal of his PhD is to optimize the foil's geometry inside a wider prospective of the boat's performance evaluated by a VPP (Velocity Prediction Program). The crucial point of the work is represented by the numerous optimization variables needed to model the foil's geometry and hydrodynamic characteristics into detail. This would entail to an incredible calculation demand and a resultant massive time-consuming process. In order to overcome this problem he makes use of automatic differentiation to obtain the differentiated version (adjoint version) of the simulation code. This adjoint code allows him to compute the gradients required for optimization around ten times faster than with conventional methods.

Finally, as far as *International Moth* is concerned, Bögle [4] and Eggert [5] did a huge work on studying the static, dynamic performance and stability with the development of a VPP and a DVPP.

1.3 International Moth Class

The International Moth is a single handed, mono hull and una-rigged dinghy. Officially the "International moth class" was born in 1972. The peculiarities of this class is stated in the opening sentence of its regulation: "*the intention of these class rules is to give the designer and builder the fullest liberty in design and construction*" [6]. The main limitations are:

- Maximum length of 3.355 m;

- Maximum beam of 2.250 ;
- Total weight is unlimited;
- Maximum sail area of $8.2 m^2$;
- Maximum overall length of mast spars of 6.250 m.



Figure 1.1: International Moth

The first Moth ever built was called 'Olivia' and was made in 1928 by *Len Morris*. After several years of development around the world, it was not until 1999 that the Australian Dr. *Ian Ward* drastically changed the class with the introduction of foils in order to lift the boat out of the water. In particular, his concept was the same as the current one. The configuration is composed by two T-foils, thus distinguishing it from catamarans and trimarans. The central T-foil consists of a vertical part called **daggerboard** and a horizontal component called **main foil**, while the rear T-foil is split into **rudder** and **rudder foil**. However, this innovation became widespread only once the main foil control system was developed by the brothers *Gath* and *John Hett*.

Another milestone in the history of the Moth was the born of the 'Bladerider' in 2005, the result of a collaboration between *McDougall*, a long-time sailor, and *McConaugh Boats*, a company specialising in composite materials. Its lightweight design, coupled with its ability to fly on water, enabled the Moth to reach record speeds and sparked great interest throughout the sailing world [7].

1.4 Thesis structure description

The thesis starts with a briefly sailing background, in chapter 2, to get the reader into the peculiarities and terminologies of the world of sailing with a specialization on the physics behind foiling boats. Then, the design tool is discussed through the underling of the mathematical aspect before going into the details of the simplified 2 DOF static model and the linearized dynamic model. Furthermore, once the boat configuration is defined, the chapter 4 aims to describe the 6 DOF dynamic model, while boat's performances, stability and manoeuvres are analysed in chapter 5 and 6.

Finally, the main results are resumed and some suggestions for the possible next steps to continue this work are indicated.

Chapter 2

Sailing Background

2.1 True and Apparent Wind

The basic concept behind sailboats is to exploiting the power of the wind by means of the sail. By interacting with the wind, the sail is capable of developing the driving force needed to move forward the boat. In static conditions, the **True Wind** is measured both in intensity TWS and direction TWA . However, as the boat speed increases, it is combined with the true wind resulting in the **Apparent Wind**. The latter is, therefore, what is actually experienced while sailing and it is responsible of the sail forces generation. The relation between true and apparent wind is stated below and it can be deduced how, as the boat's speed rise up, the AWS is more intense, while the AWA is reduced.

$$\begin{aligned} AWA &= \arccos \frac{TWS \cdot \cos(TWA) + V}{\sqrt{TWS^2 + V^2 + 2 \cdot TWS \cdot V \cos TWA}} \\ AWS &= \sqrt{TWS^2 + V^2 + 2 \cdot TWS \cdot V \cos(TWA)} \end{aligned} \quad (2.1)$$

Depending on the true wind direction, several typical courses can be identified. They are classified as Upwind courses ($TWA < 90^\circ$) and Downwind courses ($TWA > 90^\circ$):

- Close Hauled (or Windward): ($TWA \approx 40^\circ/45^\circ$);
- Beam reach (or Wind abeam): ($TWA \approx 90^\circ$);
- Reach: ($TWA \approx 100^\circ/130^\circ$);
- Broad Reach: ($TWA \approx 140^\circ/170^\circ$);
- Running (or Down-wind): ($TWA \approx 180^\circ$).

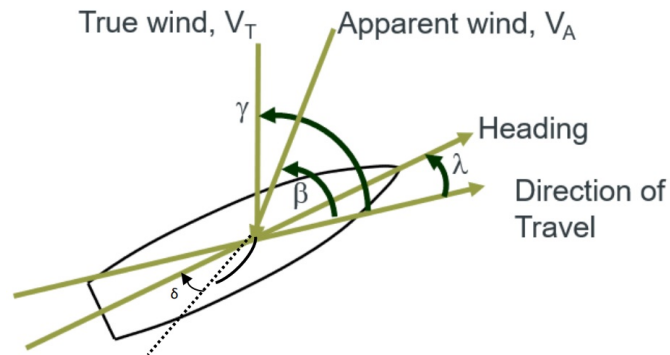


Figure 2.1: True and Apparent wind [3]

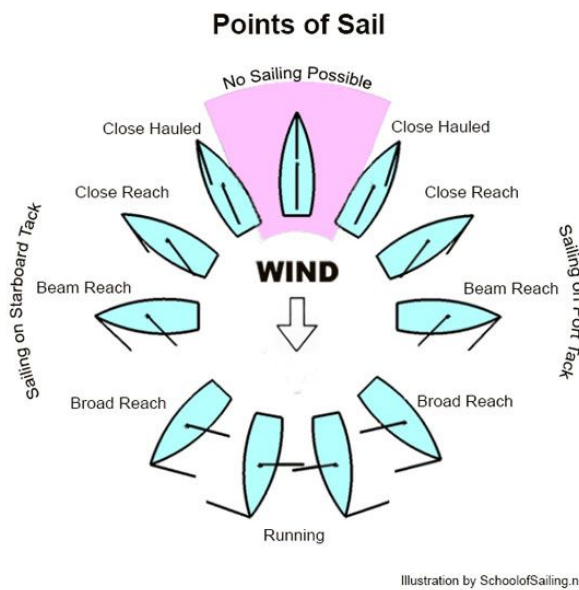


Figure 2.2: Sailing Courses [8]

Moreover, the typical manoeuvres for sailing boats, can be divided into four categories:

- **Tacking:** consists on sailing towards the wind and changing the bow direction. This is useful to go up the wind;
- **Gybing:** it is the same of Tacking for downwind courses;
- **Heading up:** consists in turning up to the wind and pass from a downwind to an upwind condition;

- **Bearing away:** consists in turning away from the wind and pass from an upwind to a downwind condition.

2.2 Physic behind

Sailing boats are complex systems because of the large number of variables involved, and the environmental interactions with air and water at the same time.

As mentioned in the last section, sail's aerodynamic forces (lift and drag) are developed by the encountering apparent wind. They are decomposed into the longitudinal and later axes, resulting in a driving force and a side force respectively. If the driving force aims to move the boat towards the desired course, the side-force prevents it, causing a lateral movement called "sway". Therefore, the direction is shifted by the "leeway angle". As a consequence, vertical appendages (daggerboard and rudder) develop hydro-dynamic forces in order to counteract the sway movement. However, these forces are responsible for the **capsizing moment** and the movement of the sailor is intended to ensure the rolling equilibrium, thus creating the '**righting moment**'. At the same time, though, it has been proved that the sailor weight is not sufficient. The sailing style of hydrofoils suggests heeling the boat windward in order to reduce the lateral force component of sail. In addition, the helmsman can act on the sail adjustments by making the sail less tight. This way, the amount of sail force decreases with the drawback of reducing the driving force too.

As far as vertical forces are concerned, the weight of sailor and the boat itself are balanced by the foils' forces. At the same time, they influence the pitching moment equilibrium. The longitudinal movements of the sailor, coupled with the control systems of the main foil and the rudder foil, are needed to ensure the balance and guarantee the desired boat's attitude.

Finally, according to the course, the aforementioned interactions can be enhanced. As depicted in figure 2.3, when sailing upwind the side-force is the dominant effect and the sailor must depower the sail. As a consequence, the maximum boat's speed in upwind course is approximately equal to the TWS. On the contrary, downwind courses are characterized by a greater driving force component and, therefore, the boat's speed can be greater than the TWS.

2.3 Main foil control system

Compared to the piercing hydrofoil boats, the *International Moth* needs the main foil control system to control, maintain ride height and ensure stability throughout the entire speed range. Since its first introduction by the brothers *Gath* and *John Hett*, the system has undergone several developments. However, the main concept is still the same: regulate the amount of lift generated by the main foil according

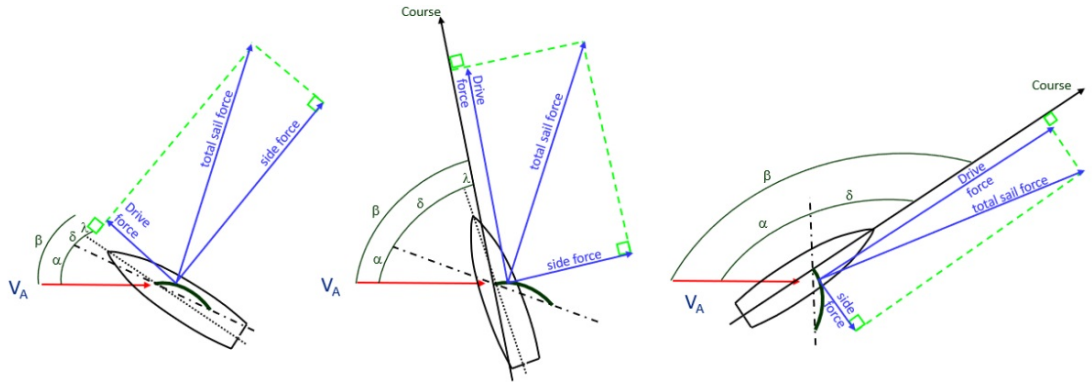


Figure 2.3: Sail Forces direction [3]

to the fly height.

In analogy with the aircrafts, this is done by moving the main foil trailing-edge flap. As a result, the AoA of the main foil changes and leads to a variation in the lift coefficient. This effect can be expressed by the derivative τ that represents the connection between the flap movement and the consequent angle of attack. Its value depends on the ratio between the flap and airfoil chords.

$$\Delta\alpha = \frac{\delta\alpha}{\delta\alpha_{flap}} \cdot \alpha_{flap} = \tau \cdot \alpha_{flap} \quad (2.2)$$

In particular, the system is based on a feedback control on the ride height given by a **sensor wand**, mounted at the bow of the boat and constantly in contact with the water surface thanks to a **rubber rope**. As the fly height changes, the wand rotates and causes the translation of the **push rod**. This latter is connected to a **bell-crack** that converts the motion from horizontal to vertical, thus moving the **flap**.

Therefore, at low rides and during the take-off phase, the flap must generate greater lift. On the other hand, when the desired ride height is reached, flap's deflection must be appropriate in order to guarantee the equilibrium condition or producing depower to prevent the boat from jumping out of the water.

The most important component that determines the performance of the system is the **bow mechanism**. Its purpose is to connect the rotation of the sensor wand, representing the current fly height, and the translation of the push rod, representing the flap movement. In the following, two of the most widespread bow mechanisms are described.

The so-called **Mach 2** [9] is composed by a pivot, consisting on a screw-nut system, directly connected to the wand by a lateral link. At the bottom, the control link provides the connection with the push rod. As a results, the rotation of the wand leads to a rotation of the pivot and consequently a translation of the push rod.

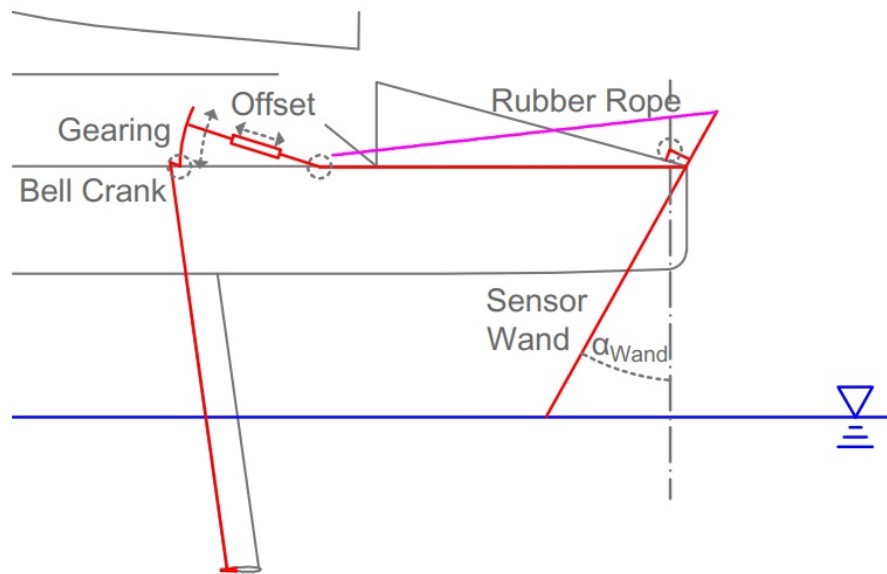


Figure 2.4: Transmission line [5]

Since the control link follows a circular trajectory, the resulting horizontal excursion is maximum when it is at the bottom, while the movement is minimum as the link goes upwards. This leads to a different sensitivity depending on the α_{wand} range. The latest control systems are mounted at the edge of a bowsprit, rather than on the deck, in order to get earlier information about disturbances, such as waves. Therefore, the system is based on the so-called **BugsCam** [10]. It differs from the **Mach 2** having a pivot that slides within a well-defined guide. The particular shape of its curve integrates the automatically change of the sensitivity and can be divided into four operating zones:

- **Zone 1:** it is active during the take off phase and aims to bring the boat to the regime condition as quickly as possible. The maximum lift is provided because the push rod takes the flap at maximum angle. The radius of curvature is almost constant and the sensitivity is small, leading to maintain the same flap angle despite a variation of the wand angle;
- **Zone 2 and 3:** they are active into the regime conditions and provide a constant sensitivity to avoid small disturbances from being transferred to the command chain;
- **Zone 4:** it is active if the right height is above the desired one, e.g. due to strong disturbances. The radius of curvature suddenly changes causing a rapid decrease of the flap angle, in order to generate sufficient depower.

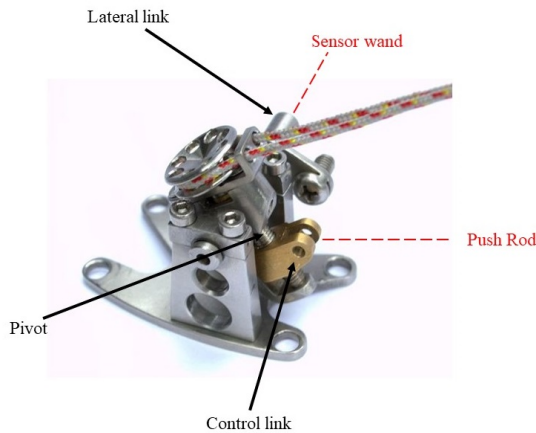


Figure 2.5: Mach 2

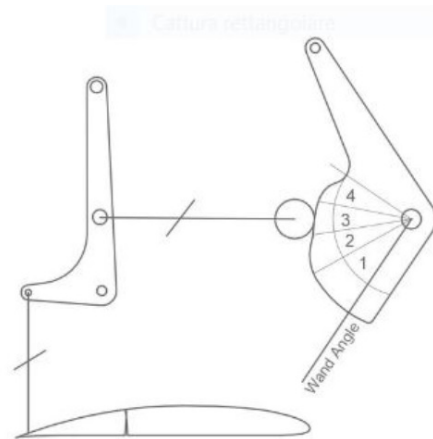


Figure 2.6: Bugs Cam

Even though the main foil control system is completely automatic, the helmsman can interact with the system by acting on different adjustments. In particular:

- **Wand length:** changing the length of the wand leads to a variation of the sensitivity of the system. In particular, if the length is reduced, the same angle swept is traduced into more translation of the push rod, thus increasing the sensitivity.
- **Offset:** it is a setting made by a screw system located on the desk and close to the daggerboard. It allows the sailor to change the zero-lift angle of flap, thus changing the desired ride height. This adjustment occurs frequently on board because, as the speed increase, the main foil would produce too much lift.
- **Gearing:** it is defined as the control of the sensitivity of flap due to variation of the wand angle. This setting is realized by changing the vertical lever arm of the bell-crank, thus changing the bell-crack ratio. This way, with the same horizontal translation of the push rod, the vertical movement is increased or decreased. Alternatively, on the **Mach2** system, this setting is done by turning the screw head and causing a variation of the length of the connection point, directly on the bow mechanism.

Chapter 3

Optimization Tool

As stated in the 1.2, the mentioned state-of-art design tools need the configuration of the boat as an input. But, what if there is no idea about it?

The first step to answer this question is to understand which are the main requirements that a racing sailboat must meet. As mentioned by Boegle [4]: “the Moth should be fast and good to handle”, therefore the high-level requirements affecting the boat’s design are:

- The boat’s configuration must maximize speed;
- The boat’s configuration must be statically stable over most of the operative range;
- The boat’s configuration must be dynamically stable over most of the operative range;
- The boat’s configuration must be manoeuvrable over most of the operative range.

These requirements has to be turned into some **performance parameters**, in order to quantify the goodness of the design itself. If maximizing speed is strictly related to the drag minimization, the concepts of stability and manoeuvrability need a more detailed investigation.

In fact, in the hydrofoiling boats and in particular on the *International Moth*, the stability is affected by several factors strongly interacting with each other. However, the main contributions come from the geometry of the boat, the control systems and the sailor’s movements and adjustments.

By analysing the real behaviour and performance of the *International Moth*, it is possible to understand how the sailor mainly affects the lateral-directional stability rather than the longitudinal one. In fact, through lateral movements and the control of the sail’s settings, the helmsman brings the boat to reach and maintain a

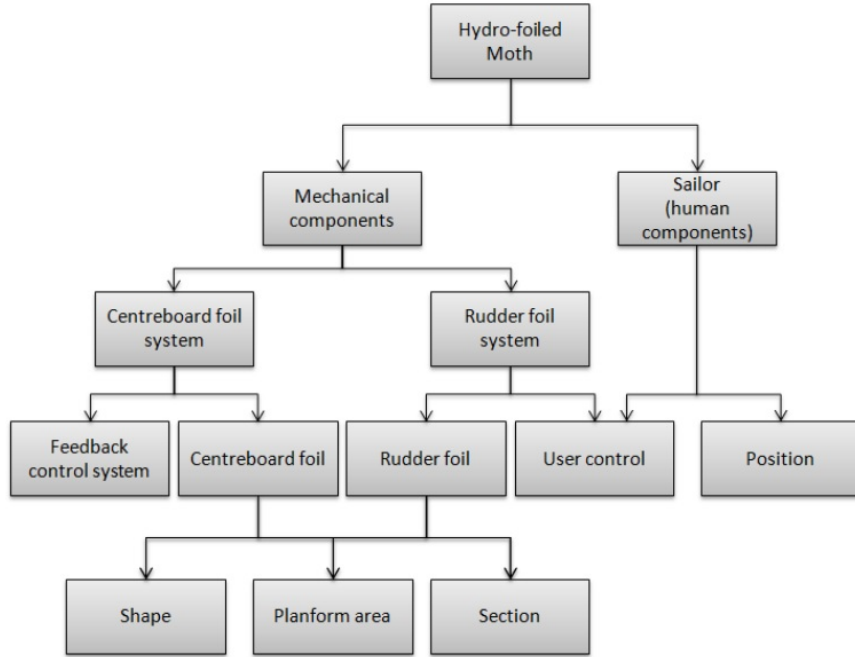


Figure 3.1: Sailor-boat interactions [4]

desired heel angle and contrasts external disturbances. Obviously, the geometry of the foils and vertical appendages also have an important effect. However, to a first approximation, the capsizing and righting moments are mainly due to the lateral force of the sail and the sailor’s weight respectively, while the effects of foils and vertical appendages can be neglected.

On the other hand, the foil’s design and the corresponding control systems play a fundamental role into the longitudinal motion. For example, different foil’s absolute surfaces would lead to a different take off and maximum speeds. Moreover, stable and unstable boats are distinguished by different surfaces distribution between main and rudder foils as well as different foil’s longitudinal positions. Therefore, the only interaction with the sailor is represented by the rudder foil control system, since the flap control is automatic.

To sum up, despite the fact that the *International Moth*’s behaviour is characterized by a strong coupling among components and therefore it is not possible to clearly distinguish causes and effects, the longitudinal motion is the one that has the greatest influence on the design. This is why, into this preliminary design phases, the simplified model is based only on the longitudinal, vertical and pitching moment equations.

Moreover, longitudinal static and dynamic stability have found wide application in

the aeronautic field. However, even though with some differences, these theories are applicable for foiling boats too.

After the evaluation of requirements through the **performance parameters**, the next step is to identify the **design variables** with which the configuration of the boat is described. From this stage follows the accuracy and the computational time of the tool. In fact, the more the **design variables** the more accurate is the definition of the geometric and hydro-dynamic characteristics and the more the optimization process is time-consuming. To find a trade-off, it is decided to represent the most relevant components of a hydrofoiling boat i.e. **foils**, because they are responsible for the boat flying and they mostly affect performances and stability.

Assuming a fixed hydro-dynamic profile, the **design variables** taken into account are the positions w.r.t the bow, the surfaces and the aspect ratios of foils:

$$(x_{mf}, x_{rf}, S_{mf}, \frac{S_{rf}}{S_{mf}}, AR_{mf}, AR_{rf}) \quad (3.1)$$

- Foils' positions (x_{mf}, x_{rf}) are related to the stability because it changes the lever arms of lift and drag forces with the respect of the centre of gravity;
- Foils' surfaces (S_{mf}, S_{rf}) are directly related to both drag and stability requirements;
- Foils' aspect ratios (AR_{mf}, AR_{rf}) , from their definition, allow to identify the geometry of foils and they affects the lifting performance and induced drag component. Therefore, AR's have an influence on both drag and stability.

To solve the problem and find the optimum combination of design variables a **genetic algorithm** is used.

Once the first boat configuration is guessed, the next step is to find the equilibrium conditions on which to evaluate the **performance parameters**. Concerning the longitudinal motion, the **state variables** are the boat's attitude θ and the fly height z . However, to get a more accurate representation of reality and of the pitching moment control, the rudder foil angle δ_R is introduced as **trim variable**. To find the equilibrium conditions a **local optimization algorithm** is implemented.

Finally, to summarise, the optimization tool aims to find the most suitable *Moth* configuration (**design variables**) to guarantee the requirements (**performance parameters**) for the whole range of operating speeds (**state variables, trim variable**), while remaining within the general limits of the project.

Some of the assumptions are resumed below and more details are provided in A.4:

- Fixed CoG position at $x_g = 2.12 \text{ m}$ from the bow;

- Fixed sailor position;
- Fixed vertical appendages' geometric and hydro-dynamic characteristics;
- Fixed centre of effort of vertical appendages;
- Fixed weight of the boat with sailor;
- Zero heel angle;
- Small leeway angle;
- Fixed foil's hydro-dynamic profile NACA 63 – 412 [11];
- Fixed vertical appendage's hydro-dynamic profile NACA 0012 [12].

3.1 Methodology

The tool can be divided into the three parts:

- User's inputs;
- Core;
- Solver.

In the first part, users can choose the operative scenario on which the boat will work, by entering the desired **speed range**. Then, it is asked to decide the design variables involved into the optimization process, and finally, setting the **boundaries** on within which the design can move.

The **core** of the tool is the model of the boat whereby the performance parameters can be evaluated. Surrounding the whole, the **solver** is capable of finding the best boat's configuration and calculate its equilibrium conditions within the operative range.

After entering the necessary inputs, the **genetic algorithm** is started, in order to generate the first guess of boat's configuration. At this point, there is the need to understand if this configuration meets the requirements or not. For this purpose, the **local solver** receives the geometry as an input and finds the equilibrium solution for every speed considered. Subsequently, the performance parameters are evaluated in order to write the **objective function** that the genetic algorithm aims to minimize. This process is repeated and, by the end, the tool provides the optimum boat's configuration among those guessed, with the corresponding equilibrium conditions.

In order to guarantee a feasible solution, the design space is limited by two constrains:

- Take off: it is imposed that the 70% of the boat's weight is withstand by the main foil at the take off speed. This condition has a direct consequence on the minimum value of main foil surface that the optimization toll can handle:

$$L_{mf_{TO}} \geq 0.7 \cdot W \longrightarrow S_{mf} \geq \frac{2 \cdot 0.7 \cdot W}{\rho V_{TO}^2 C_{L_{TO}}} \quad (3.2)$$

- Stall preventing: this condition comes from the aeronautic field concerning the design of the horizontal tail. It is imposed that the stall angle of the rudder foil is greater than the one of the main foil. This way, it would be possible to recover from a critical condition and prevent the boat to collapse because of the stall of the main foil. This constraint affects the value of the aspect ratio as follows:

$$AR_{rf} \geq AR_{mf} \quad (3.3)$$

Moreover, boundaries on the absolute values of the design variables are stated in the table below:

$x_{mf}[m]$	$x_{rf}[m]$	$S_{mf}[m^2]$	$\frac{S_{rf}}{S_{mf}}[-]$	$AR_{mf}[-]$	$AR_{rf}[-]$
1.3 ÷ 1.5	3.3 ÷ 3.8	0.08 ÷ 0.14	0.4 ÷ 0.82	7 ÷ 11	7 ÷ 11

Table 3.1: Boundaries on design variables

As far as the **objective function** is concerned, it consists on a weighted average of the total amount of drag and the value of the pitching moment derivative. However, since the tool aims to find the optimum configuration among the entire speed range, the total objective function is given by the sum of the partial ones.

$$obj_{function} = \sum \left(K_1 \cdot Drag(i) + K_2 \cdot C_{M_\alpha}(i) \right) \quad (3.4)$$

The dynamic stability is evaluated through the eigenvalues coming from the linearized model. Nevertheless, due to the difficulty in expressing them as part of the objective function, it is decided to penalise the “unstable population” of design variables and rule them out from the selection.

3.2 Static Model

As previously mentioned, the model of the boat composes the core of the tool. Although the full dynamic model will be presented in the following chapters (4), at this stage there is a need to simplify the model, highlighting the most important features and avoiding an extreme time-consuming process. Hence, the development

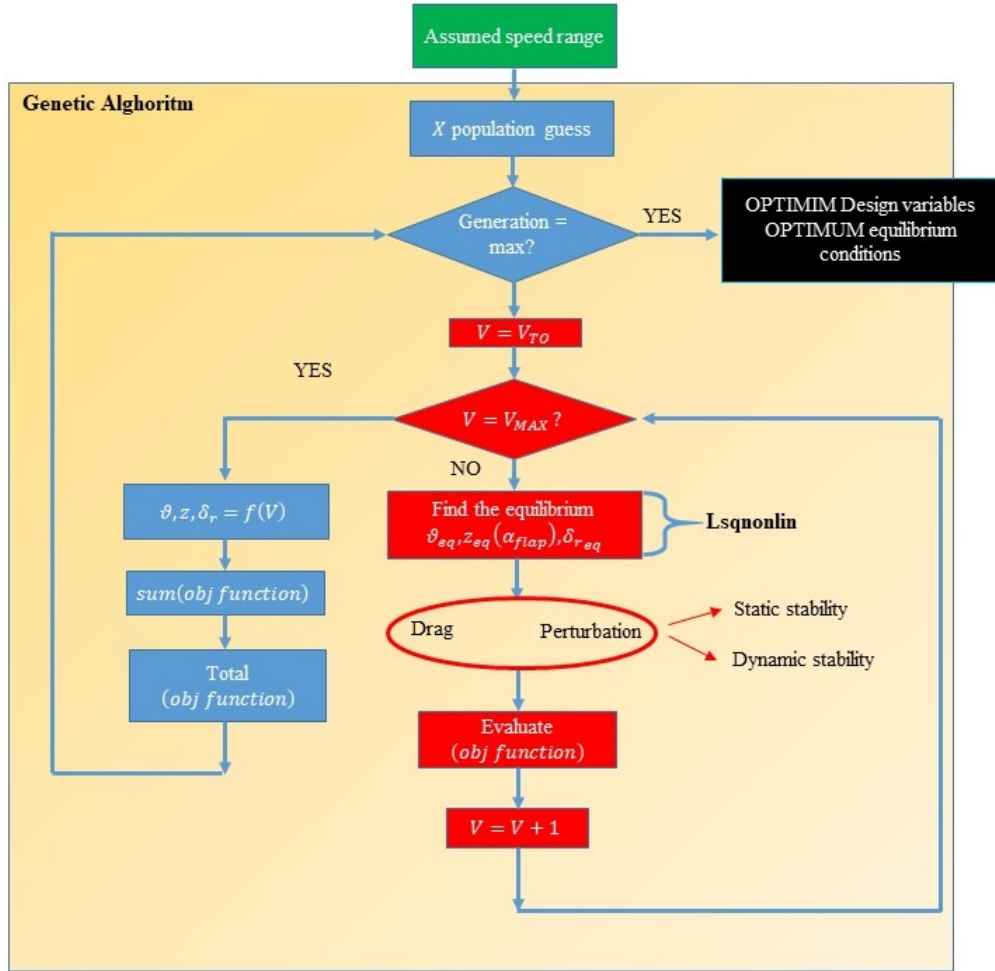


Figure 3.2: Algorithm flow chart

of a static 2 DOF model focusing on the longitudinal motion. Since the input of the model is the speed range, it is assumed the longitudinal equilibrium equation is already satisfied by imposing that the driving sail force is equal to the sum of drags. Consequently, the two degrees of freedom taken into account regard the vertical equilibrium and the pitching moment equilibrium. The state variables representing the system are the boat's **attitude** θ and the boat's **fly height** z and the **rudder foil angle** δ_R is the trim variable.

The model description starts with the definition of the reference systems. They follow the aeronautic convention for the axes orientation: longitudinal axes towards the bow, vertical axes towards the water surface and the lateral one as a consequence.

In particular, the frames are:

- **BODY**: follows the boat's movements and the equilibrium equations are written into this reference system.
- **INERTIAL**: fixed reference system. By comparing with the body frame, the state variables are identified.

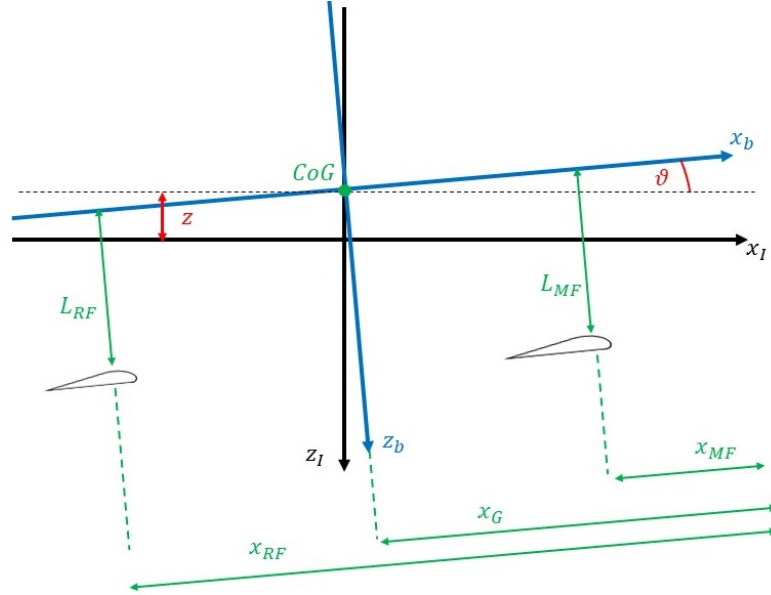


Figure 3.3: Reference frames 2 DOF model

The classic aerodynamic theory is used to express lift and drag forces and typical foiling boat's phenomena like the free-surface and the wave drag effects are taken into account.

$$\begin{aligned} L &= \frac{1}{2} \rho V^2 S C_L \\ D &= \frac{1}{2} \rho V^2 S C_D \end{aligned} \quad (3.5)$$

The free-surface effect is responsible of the worsening of the lifting performance, as the foil is closer to the water surface. In particular, there is an inflow speed reduction as well as the effective profile chamber decreases. Through the biplane analogy, is possible to obtain an analytical expression of the free-surface correction [13]:

$$C_L = C_{L\infty} \cdot (1 - 0.422 \cdot e^{-1.454 \cdot \frac{h}{c}}) \quad (3.6)$$

The second effect is related to the wave generation [3] and therefore, another drag component is added to the shape drag and the induced drag:

$$C_D = C_{D_0} + C_{D_i} + C_{D_{wv}} \quad (3.7)$$

$$C_{D_{wv}} = \frac{1}{2} \cdot K_0 \cdot c \cdot C_L^2 \cdot e^{-2K_0 h} \quad (3.8)$$

After the force modules calculation into the inertial frame, they are converted into the body axes by using the rotational matrix Θ , representing the rotation around the y_b axes:

$$\Theta = \begin{bmatrix} \cos \theta & 0 & \sin \theta \\ 0 & 1 & 0 \\ -\sin \theta & 0 & \cos \theta \end{bmatrix} \quad (3.9)$$

Finally, the equilibrium equations are stated:

$$\begin{cases} F_z = 0 \\ M_y = 0 \end{cases} \quad (3.10)$$

As underlined in the 3.1, the local optimization algorithm aims to solve the system of these two equations. However, the problem has three unknowns, which are the two state variables and the rudder foil angle. For this purpose, another condition is added: the attitude of a *Moth* must be as neutral as possible. This statement, coming from observation, allows the optimization to find an equilibrium condition in line with the real behaviour of the boat. Therefore, the local optimization algorithm is asked to solve the following problem:

$$\begin{cases} F_z = 0 \\ M_y = 0 \\ \theta = 0 \end{cases} \quad (3.11)$$

As done with the genetic algorithm, boundaries on the state variables are imposed.

θ [deg]	z [m]	δ_R [deg]
-3 ÷ 2	0 ÷ 0.8	-6 ÷ 3

Table 3.2: Boundaries on state variables

3.3 Static Stability Evaluation

The static stability concept stems from the aeronautic field. An aircraft flying in an equilibrium condition, is statically stable if, following an external disturbance, it is able to return to the previous condition. Similarly, the same concept is applicable for the foiling boat, albeit with some differences. Indeed, the stability problem of an aircraft can be approximated by considering only the linear terms, i.e. those taking into account the lift forces ($C_L = f(\alpha)$). On the contrary, the moth configuration envisages two long vertical appendages (daggerboard and rudder) causing the fluid dynamic forces to be applied at a significant distance with the respect to the centre of gravity. This way, the moment due to drag forces cannot be neglected and the problem cannot be linearized ($C_D = f(\alpha^2)$).

The longitudinal static stability is assessed by introducing the derivative of pitching moment's coefficient [14]. Starting from the previous model is possible to simulate a small perturbation by evaluating M_y at a fixed speed and with different boat's attitudes. At this point, the pitching moment coefficient is calculated by normalizing with the respect of the main foil:

$$C_M = \frac{M_y}{\frac{1}{2}\rho V^2 S_{mf} c_{mf}} \quad (3.12)$$

Finally, it is possible to calculate the derivative $C_{M\alpha}$ in the equilibrium point. This is done by approximating the C_M curve with a linear interpolation, resulting in:

$$C_M = C_{M_0} + C_{M\alpha} \cdot \theta \quad (3.13)$$

3.4 Dynamic Stability: linearized model

With the aim of moving the first step into the dynamic aspects of the design, the linearized dynamic model is developed. If static stability concerns the boat's **first reaction** after a perturbation, dynamic stability takes into account **how** the boat tends to return to its previous equilibrium condition. This dynamic behaviour is crucial in sailboat design because there are simultaneous perturbations and the boat must be able to mitigate these effects. In addition, the sailor himself can cause an external disturbance on the system by making some small mistakes. In this case, it is necessary for the boat to be "forgiving" and allows the sailor to continue the regatta without critical consequences.

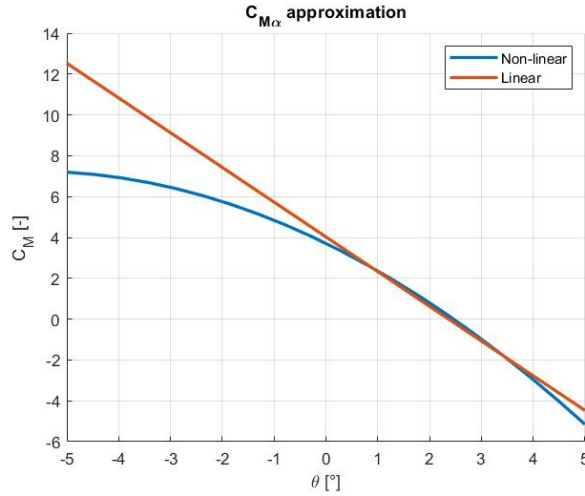


Figure 3.4: $C_{M\alpha}$ linear approximation

3.4.1 Small perturbation theory

The dynamic stability is analysed through the small perturbation theory. As a result, the equations can be linearized and the state space formulation is obtained:

$$\begin{cases} \dot{\bar{x}} = A\bar{x} + B\bar{u} \\ \bar{y} = C\bar{x} + D\bar{u} \end{cases} \quad (3.14)$$

The dynamic characteristic of the system depends on the state matrix only. Moreover, the aim of the optimization tool is to find the boat's configuration that is **intrinsically stable** without the involvement of external controls. For this reason, the command vector is not taken into account. The second equation represents the “output equation” and it is not useful for evaluating the dynamic behaviour.

In particular, the equation $\dot{\bar{x}} = A\bar{x}$ identifies a system of n first order homogenous differential equations and can be solved with the eigenvalue's theory. The free response of the system, starting from an initial condition, depends on the **eigenvalues** and **eigenvectors** of the state matrix A . Through the modal decomposition technique, the time response is stated [14]:

$$\bar{x}(t) = \sum \bar{V}_i \cdot [\bar{W}_i^T \cdot \bar{x}_0] \cdot e^{\lambda_i t} \quad (3.15)$$

The eigenvalues indicate the modal response and their sign determines the stability or instability of the system, while the eigenvectors represent the relationship among the state variables i.e. the mode shape.

As far as eigenvalues are concerned, they are calculated by solving the characteristic

equation $\det(A - \lambda I) = 0$ and they can be real or complex and conjugate numbers leading to an aperiodic or oscillatory mode respectively:

$$\lambda = a \quad \lambda = a \pm jb \quad (3.16)$$

If the real part is negative, the system is stable because it conjugate back to the previous condition; on the other hand it will diverge. The imaginary part is the frequency of the damped system and it is strictly related to the oscillation period:

$$e^{\lambda t} = e^{(a \pm jb)t} = e^{at} (\cos(bt) \pm j \sin(bt)) \quad (3.17)$$

In order to evaluate the main characteristics of the modal response, some parameters are listed below. Finally, the graphic tool of the **Root Loci** is used to depict

Damped frequency [rad/s]	$\omega = b = \text{Im}(\lambda)$
Damping factor [-]	$\zeta = -\frac{a}{\omega_n}$
Natural system frequency [rad/s]	$\omega_n = \frac{\omega}{\sqrt{1-\zeta^2}}$
Oscillation period [s]	$T = \frac{2\pi}{\omega}$
Decay time [s]	$t_{1/2} = \frac{\ln(2)}{a}$
Decay cycles [-]	$N_{1/2} = \frac{t_{1/2}}{T}$

Table 3.3: Parameters of modal response

eigenvalues and their evolution with the system's parameters. Circular lines represents iso-frequency curves that increase its radius as the system's response is faster, whereas the radial lines concern iso-damping conditions and, as they get closer to the real axis, the greater the damping.

The connection between static and dynamic stability can be stated by the second Routh criteria [14]: “*a system can be statically stable but dynamically unstable. On the other hand, if the dynamic stability is guaranteed, so the static stability*”. These sentences are resumed into the **Stability Diagram** which relates the static and dynamic stability through the C_{M_α} and the real part of eigenvalues respectively. In particular:

- First quadrant: dynamically and statically stable conditions;
- Second quadrant: dynamically stable but statically unstable conditions;
- Third quadrant: dynamically unstable and statically unstable conditions;
- Fourth quadrant: dynamically unstable but statically stable conditions.

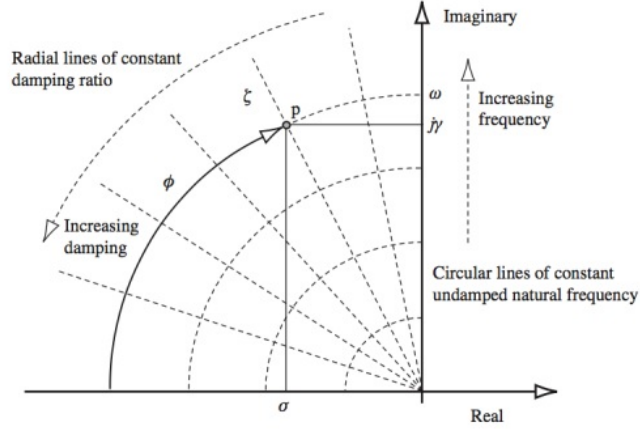


Figure 3.5: Root Loci [14]

3.4.2 Longitudinal stability

As far as the optimization tool is concerned, the interest of the problem is on the longitudinal dynamic. Therefore, the following **state variables** can be identified:

$$\bar{x} = \{u, w, \theta, q, h\}^T \quad (3.18)$$

The equilibrium equations are referred to the body reference frame. However, the equilibrium system is then completed with two kinematic equations regarding the pitch angle rate and the vertical speed into the inertial reference system [13]:

$$\begin{cases} m\dot{u} = F_x \\ m(\dot{w} - Vq) = F_z \\ I_y\dot{q} = M_y \\ q = \dot{\theta} \\ \dot{h} = w - V\theta \end{cases} \quad (3.19)$$

Furthermore, the linearization occurs into the forces and moments expressions, assuming a small leeway angle and a zero heel angle. They are written with a linear Taylor series expansion, thus introducing the **stability derivatives**, as function of state variables:

$$F_x = X_u u + X_w w + X_\theta \theta + X_q q + X_h h \quad (3.20)$$

$$F_z = Z_u u + Z_w w + Z_\theta \theta + Z_q q + Z_h h + Z_{\dot{w}} \dot{w} + Z_{\dot{q}} \dot{q} \quad (3.21)$$

$$M_y = M_u u + M_w w + M_\theta \theta + M_q q + M_h h + M_{\dot{w}} \dot{w} + M_{\dot{q}} \dot{q} \quad (3.22)$$

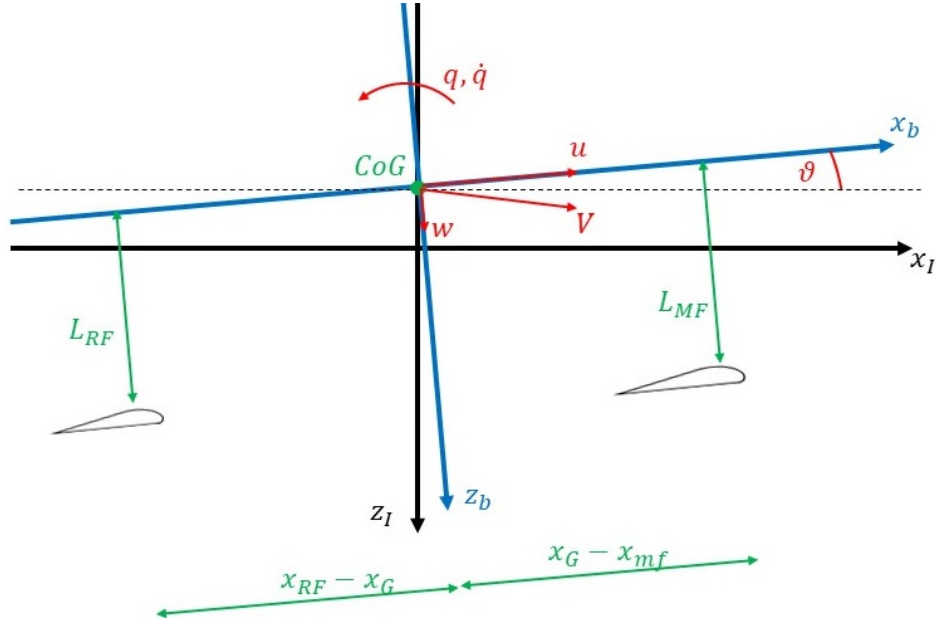


Figure 3.6: Reference frame and state variables

Finally, from the equations 3.19, the state space matrix is obtained.

$$\begin{Bmatrix} \dot{u} \\ \dot{w} \\ \dot{\theta} \\ \dot{q} \\ \dot{h} \end{Bmatrix} = \begin{bmatrix} \frac{X_u}{m} & \frac{X_w}{m} & \frac{X_\theta}{m} & \frac{X_q}{m} & \frac{X_h}{m} \\ \frac{Z_u}{m-Z_{\dot{w}}} & \frac{Z_w}{m-Z_{\dot{w}}} & \frac{Z_\theta}{m-Z_{\dot{w}}} & \frac{Z_q+m\theta_{eq}}{m-Z_{\dot{w}}} & \frac{Z_h}{m-Z_{\dot{w}}} \\ 0 & 0 & 0 & 1 & 0 \\ \frac{M_u}{I_y-M_{\dot{q}}} & \frac{M_w}{I_y-M_{\dot{q}}} & \frac{M_\theta}{I_y-M_{\dot{q}}} & \frac{M_q}{I_y-M_{\dot{q}}} & \frac{M_h}{I_y-M_{\dot{q}}} \\ 0 & 1 & -V_{eq} & 0 & 0 \end{bmatrix} \cdot \begin{Bmatrix} u \\ w \\ \theta \\ q \\ h \end{Bmatrix} \quad (3.23)$$

3.4.3 Derivatives

The **stability derivatives** take into account how forces and moments will change following a small disturbance. Their expressions are combination of the **elementary derivatives** and depend on the geometry of the boat as well as the equilibrium condition considered.

As mentioned in section 2.3, the main foil control system is the key to guarantee the longitudinal stability. By analysing the system transmission from the sensor wand to the flap angle, it possible to identify the evolution of the flap angle as function of the ride height. It is approximated by a quadratic interpolation to simplify the expression and facilitate the calculation of the derivative. As the ride height decreases, the flap angle increases to generate more lift and return to the previous condition. This results in a negative value of the derivative $\frac{\delta\alpha_{flap}}{\delta z}$. However, the state variable is the submerged length and not the ride height, so if

the boat tends to fall down, the submerged length is greater. The minus sign is therefore necessary to describe this opposite dependency:

$$\alpha_{flap} = P_1 + P_2 z + P_3 z^2 \quad (3.24)$$

$$\frac{\delta \alpha_{flap}}{\delta h} \Big|_{eq} = \frac{\delta \alpha_{flap}}{\delta z} \frac{\delta z}{\delta h} = - \frac{\delta \alpha_{flap}}{\delta z} \Big|_{eq} = -(P_2 + 2P_3 z_{eq}) \quad (3.25)$$

Lift and drag coefficients are function of:

- AoA, through the hydro-dynamic characteristics of foils i.e. lift curve slope $C_{L\alpha}$;
- Ride height, due to the free surface and wave drag effects.

In particular, the derivatives w.r.t AoA are the same for main foil and rudder foil, while there is a great difference when evaluating them as function of the ride height. In fact, the main foil's derivative takes into account the flap angle variation, which has a huge impact on its sign and value. On the contrary, the rudder foil control system is not related to the fly height.

$$\frac{\delta C_{Lmf}}{\delta \alpha} \Big|_{eq} = a_{mf} \cdot (1 - 0.422 e^{-1.454 \frac{h_{eq}}{c}}) \quad (3.26)$$

$$\frac{\delta C_{Lrf}}{\delta \alpha} \Big|_{eq} = a_{rf} \cdot (1 - 0.422 e^{-1.454 \frac{h_{eq}}{c}}) \quad (3.27)$$

$$\begin{aligned} \frac{\delta C_{Lmf}}{\delta h} \Big|_{eq} &= \frac{\delta C_{L\infty}}{\delta h} + C_{L\infty} \left(\frac{1.454 \cdot 0.422}{c} e^{-1.454 \frac{h_{eq}}{c}} \right) = \\ &= a_{mf} \tau \frac{\delta \alpha_{flap}}{\delta h} \Big|_{eq} \cdot (1 - 0.422 e^{-1.454 \frac{h_{eq}}{c}}) + \\ &+ a_{mf} (\theta + i_{mf} + \tau \alpha_{flap}) \left(\frac{1.454 \cdot 0.422}{c} e^{-1.454 \frac{h_{eq}}{c}} \right) \end{aligned} \quad (3.28)$$

$$\frac{\delta C_{Lrf}}{\delta h} \Big|_{eq} = a_{rf} (\theta_{eq} + i_{rf} + \delta_{req}) \left(\frac{1.454 \cdot 0.422}{c} e^{-1.454 \frac{h_{eq}}{c}} \right) \quad (3.29)$$

As far as drag coefficient is concerned, only the induced drag, which includes the derivatives $\frac{\delta C_L}{\delta h}$, and the wave drag components vary with the AoA and the ride height. The following expressions are valid for both the main foil and rudder foil:

$$\frac{\delta C_D}{\delta \alpha} \Big|_{eq} = \frac{\delta (C_{D0} + C_{Di} + C_{D_{wv}})}{\delta \alpha} = \frac{2C_{Leq}}{e\pi AR} \frac{\delta C_L}{\delta \alpha} \Big|_{eq} + K_0 \cdot c \cdot C_{Leq} \frac{\delta C_L}{\delta \alpha} \Big|_{eq} e^{-2K_0 h_{eq}} \quad (3.30)$$

$$\begin{aligned}
 \frac{\delta C_D}{\delta h} \Big|_{eq} &= \frac{\delta(C_{D_0} + C_{D_i} + C_{D_{wv}})}{\delta h} = \\
 &= \frac{2C_{L_{eq}}}{e\pi AR} \frac{\delta C_L}{\delta h} \Big|_{eq} + \frac{1}{2} K_0 c \left(2C_{L_{eq}} \frac{\delta C_L}{\delta h} \Big|_{eq} e^{-2K_0 h_{eq}} + C_{L_{eq}}^2 (-2K_0) e^{-2K_0 h_{eq}} \right)
 \end{aligned} \tag{3.31}$$

From the latter expressions, some considerations on the sign and values of the derivatives are discussed.

The lift coefficient derivatives w.r.t AoA are always positive, while the drag derivatives are strictly dependent on the equilibrium condition, i.e. depend on the sign of the AoA. Then, $\frac{\delta C_{L_{mf}}}{\delta h}$ has a positive value because of the two effects of flap and free surface. In particular, if the foil is further from the water surface, the lifting performance are improved and the flap angle is increased too. As far as rudder foil is concerned, the behaviour is the same, but it is more likely to have a negative $C_{L_{rf}}|_{eq}$ resulting in a negative value of $\frac{\delta C_{L_{rf}}}{\delta h}$.

Finally, the drag variation with the fly height has two opposite contributes. If the wave drag would lead to a decrease of the drag coefficient as the submerged length increases, the induced component causes an opposite effect due to the increase of the lift coefficient. This latter contribution is more relevant in the main foil because of the flap angle effect.

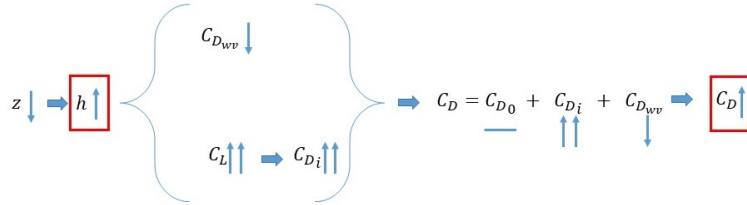


Figure 3.7: Derivatives contributions

At this point, the **stability derivatives** are described, investigating the effect of the variations of the state variables on forces and moments. It is worth noticing that the body reference system follows the aeronautic convection with the vertical axes towards the water. Therefore, in the following, a rise of lift leads to a negative increase of vertical force F_Z , and a rise of drag leads to negative increase of longitudinal force F_X . Moreover, from the assumption of small leeway angle, the only force considered on the vertical appendages is the drag. In particular, it is function of the longitudinal speed and the submerged surface variation through the derivative $\frac{\delta S}{\delta h}$.

- u derivatives: the more the speed, the more drag and lift, while the effect on the pitching moment is null:

$$\begin{aligned} X_u &= -\rho V_{eq} (S_{mf} C_{D_{mf}} + S_{rf} C_{D_{rf}} + S_D C_{D_D} + S_R C_{D_R}) \\ Z_u &= -\rho V_{eq} (S_{mf} C_{L_{mf}} + S_{rf} C_{L_{rf}}) \\ M_u &= 0 \end{aligned} \quad (3.32)$$

- w derivatives: they take into account the variation of the angle of attack due to the composition of the vertical speed with the longitudinal one: $\Delta\alpha = \frac{w}{u}$ (figure 3.8). The longitudinal resultant is increased ($X_w > 0$) because there is a positive lift component on the x_b direction. The magnitude of the vertical resultant is increased ($Z_w < 0$) because there is a positive drag component in the z_b direction. This is called "**lifting damping effect**" because, as the boat tends to go up ($w < 0$), the amount of lift is damped by the reduction of the angle of attack. The pitching moment is composed by a positive component of the main foil's lift, while the rudder foil's lift and drags lead to a negative contribution ($M_w < 0$):

$$\begin{aligned} X_w &= \frac{1}{2} \rho V_{eq} (S_{mf} C_{L_{mf}} + S_{rf} C_{L_{rf}}) - \frac{1}{2} \rho V_{eq} (S_{mf} C_{D_{\alpha_{mf}}} + S_{rf} C_{D_{\alpha_{rf}}}) \\ Z_w &= -\frac{1}{2} \rho V_{eq} (S_{mf} C_{D_{mf}} + S_{rf} C_{D_{rf}} + S_D C_{D_D} + S_R C_{D_R}) + \\ &\quad - \frac{1}{2} \rho V_{eq} (S_{mf} C_{L_{\alpha_{mf}}} + S_{rf} C_{L_{\alpha_{rf}}}) \\ M_w &= \frac{1}{2} \rho V_{eq} S_{mf} (C_{D_{mf}} + C_{L_{\alpha_{mf}}}) l_{x_{mf}} - \frac{1}{2} \rho V_{eq} S_{rf} (C_{D_{rf}} + C_{L_{\alpha_{rf}}}) l_{x_{rf}} + \\ &\quad + \frac{1}{2} \rho V_{eq} S_{mf} (C_{L_{mf}} - C_{D_{\alpha_{mf}}}) l_{z_{mf}} + \frac{1}{2} \rho V_{eq} S_{rf} (C_{L_{rf}} - C_{D_{\alpha_{rf}}}) l_{z_{rf}} \end{aligned} \quad (3.33)$$

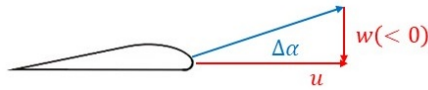


Figure 3.8: Vertical speed effect

- θ derivatives: they take into account how the boat reacts after changing its attitude. A pitch angle produces a component of the weight into the longitudinal axes and changes the submerged length of the two foils leading to a variation in the lifting and resistance performance. In particular, if $\theta > 0$, the

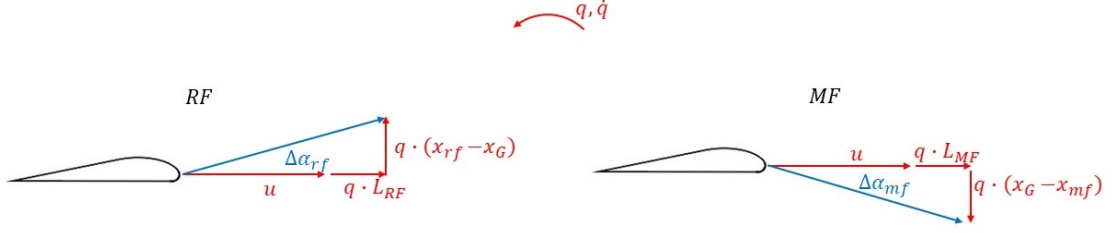
longitudinal resultant is negative ($X_\theta < 0$) because of the weight component $-W\theta$. The main foil is closer to the free surface leading to a less $C_{L_{mf}}$, while the rudder foil is further and the $C_{L_{rf}}$ is thus increased. These result to a lowering of the boat ($Z_\theta > 0$). The pitching moment tends to be negative ($M_\theta < 0$) because of the latter trends of foils' lift:

$$\begin{aligned}
 X_\theta &= \frac{1}{2}\rho V_{eq}^2 \left(S_{mf} C_{D_{h_{mf}}} l_{x_{mf}} - S_{rf} C_{D_{h_{rf}}} l_{x_{rf}} \right) - W \\
 Z_\theta &= \frac{1}{2}\rho V_{eq}^2 \left(S_{mf} C_{L_{h_{mf}}} l_{x_{mf}} - S_{rf} C_{L_{h_{rf}}} l_{x_{rf}} \right) \\
 M_\theta &= \frac{1}{2}\rho V_{eq}^2 \left(S_{mf} C_{D_{h_{mf}}} l_{x_{mf}} l_{z_{mf}} - S_{rf} C_{D_{h_{rf}}} l_{x_{rf}} l_{z_{rf}} + \right. \\
 &\quad \left. - S_{mf} C_{L_{h_{mf}}} l_{x_{mf}}^2 - S_{rf} C_{L_{h_{rf}}} l_{x_{rf}}^2 \right)
 \end{aligned} \tag{3.34}$$

- q derivatives: they take into account another damping effect. A pitch rate results in a linear velocity perturbation along longitudinal and vertical axes. The latter can be traced back to the effect of the vertical speed w . In particular, considering figure 3.9, with a positive increment of the pitch rate, the velocity of main foil and rudder foil is increased by qz . At the same time, the angle of attack of main foil is decreased by $-\frac{ql_{x_{mf}}}{u}$, while the angle of attack of rudder foil is increased by $\frac{ql_{x_{rf}}}{u}$ leading to a negative pitching moment ($M_q < 0$):

$$\begin{aligned}
 X_q &= -\rho V_{eq} \left(S_{mf} C_{D_{mf}} l_{z_{mf}} + S_{rf} C_{D_{rf}} l_{z_{rf}} + S_D C_{D_D} l_{z_D} + S_R C_{D_R} l_{z_R} \right) + \\
 &\quad + \frac{1}{2}\rho V_{eq} \left(S_{mf} C_{D_{\alpha_{mf}}} l_{x_{mf}} - S_{rf} C_{D_{\alpha_{rf}}} l_{x_{rf}} \right) \\
 Z_q &= -\rho V_{eq} \left(S_{mf} C_{L_{mf}} l_{z_{mf}} + S_{rf} C_{L_{rf}} l_{z_{rf}} \right) + \\
 &\quad + \frac{1}{2}\rho V_{eq} \left(S_{mf} C_{L_{\alpha_{mf}}} l_{x_{mf}} - S_{rf} C_{L_{\alpha_{rf}}} l_{x_{rf}} \right) \\
 M_q &= -\frac{1}{2}\rho V_{eq} \left(2C_{D_{mf}} l_{z_{mf}} - C_{D_\alpha} l_{x_{mf}} \right) S_{mf} l_{z_{mf}} + \\
 &\quad + \frac{1}{2}\rho V_{eq} \left(2C_{L_{mf}} l_{z_{mf}} - C_{L_\alpha} l_{x_{mf}} \right) S_{mf} l_{x_{mf}} + \\
 &\quad - \frac{1}{2}\rho V_{eq} \left(2C_{D_{rf}} l_{z_{rf}} - C_{D_\alpha} l_{x_{rf}} \right) S_{rf} l_{z_{rf}} + \\
 &\quad - \frac{1}{2}\rho V_{eq} \left(2C_{L_{rf}} l_{z_{rf}} - C_{L_\alpha} l_{x_{rf}} \right) S_{rf} l_{x_{rf}}
 \end{aligned} \tag{3.35}$$

- h derivatives: they take into account how lift and drag changes with the submerged length. As described with the elementary derivatives, the main


Figure 3.9: Pitch rate effect

contribution is given by the flap angle leading to an increase of drag and lift ($X_h < 0, Z_h < 0$). At the same time, the boat tends to pitch up because the greater lift on the main foil ($M_h < 0$).

$$\begin{aligned}
 X_h &= -\frac{1}{2}\rho V_{eq}^2 (S_{mf} C_{D_{h_{mf}}} + S_{rf} C_{D_{h_{rf}}} + S_{h_D} C_{D_D} + S_{h_R} C_{D_R}) \\
 Z_h &= -\frac{1}{2}\rho V_{eq}^2 (S_{mf} C_{L_{h_{mf}}} + S_{rf} C_{L_{h_{rf}}}) \\
 M_h &= -\frac{1}{2}\rho V_{eq}^2 (S_{mf} C_{D_{h_{mf}}} l_{z_{mf}} + S_{rf} C_{D_{h_{rf}}} l_{z_{rf}} + S_{h_D} C_{D_D} l_{z_D} + S_{h_R} C_{D_R} l_{z_R}) + \\
 &\quad + \frac{1}{2}\rho V_{eq}^2 (S_{mf} C_{L_{h_{mf}}} l_{x_{mf}} - S_{rf} C_{L_{h_{rf}}} l_{x_{rf}})
 \end{aligned} \tag{3.36}$$

- \dot{w} derivatives: they take into account the **added mass effect** of foils along the vertical direction. With the approximation of considering the foil surface as elliptic, the derivatives are obtained as function of the inertia factors (K_{mf}, K_{rf}) given by [15]:

$$\begin{aligned}
 X_{\dot{w}} &= 0 \\
 Z_{\dot{w}} &= -\rho \frac{\pi}{4} (K_{mf} S_{mf} c_{mf} + K_{rf} S_{rf} c_{rf}) \\
 M_{\dot{w}} &= \rho \frac{\pi}{4} (K_{mf} S_{mf} c_{mf} l_{x_{mf}} - K_{rf} S_{rf} c_{rf} l_{x_{rf}})
 \end{aligned} \tag{3.37}$$

- \dot{q} derivatives: they take into account the **added mass effect** due to the pitching acceleration. Similarly to the previous ones, the derivatives are:

$$\begin{aligned}
 X_{\dot{q}} &= 0 \\
 Z_{\dot{q}} &= \rho \frac{\pi}{4} (K_{mf} S_{mf} c_{mf} x_{mf} - K_{rf} S_{rf} c_{rf} x_{rf}) \\
 M_{\dot{q}} &= -\rho \frac{\pi}{4} (K_{mf} S_{mf} c_{mf} l_{x_{mf}}^2 + K_{rf} S_{rf} c_{rf} l_{x_{rf}}^2)
 \end{aligned} \tag{3.38}$$

3.5 Results

In this section the optimization tool's results are presented. Simulations are carried out by assuming a take-off speed of 3.5 m/s and a maximum speed of 11.5 m/s . As far as the take-off condition constraint is concerned, the most demanding case was taken into account. In fact, in order to emphasize the importance of the main foil's surface, the minimum value of lift coefficient was selected by considering a null pitch angle and the minimum value of aspect ratio. The latter results in $C_{L_{mf@TO}} \approx 1$.

The **genetic algorithm** [16] is started with the Matlab default settings consisting of 100 as number of maximum iterations and 200 as maximum population size. For the objective function, after several attempts, the weighting parameters K_1 and K_2 are set to 400 and 1.5 respectively. The reason lies on the definition of the two performance parameters: pseudo drag coefficient $C_{D_{pseudo}}$ and derivative of pitching moment C_{M_α} .

$$C_{D_{pseudo}} = \frac{Drag}{\frac{1}{2}\rho V^2} \quad (3.39)$$

From a preliminary estimate of their order of magnitude, it is possible to assess $C_{D_{pseudo}} \approx 0.01[m^2]$ and $C_{M_\alpha} \approx 1[1/^\circ]$. Therefore, the objective function at each speed amounts to about 5.5.

$$obj_{function}(i) = K_1 \cdot C_{D_{pseudo}}(i) + K_2 \cdot C_{M_\alpha}(i) \approx 5.5 \quad (3.40)$$

Finally, the **local optimization algorithm** was implemented by the Matlab default routine called **MultiStart** [17], aiming to find the equilibrium system's solution with a tolerance of $1 \cdot 10^{-4}$.

The genetic algorithm converges towards the minimum value of the objective function. As a consequence, the optimization process results in an optimum configuration of the boat in line with the commercial ones, despite some differences. The longitudinal foils' position certifies the algorithm's goal towards stability. In fact, the rudder foil is placed at 3.8 m to maximize the pitching down moment. On the other hand, the main foil position is closer to the upper limit of the design space (1.53 m), resulting in a smaller arm relative to the centre of gravity and, consequently, a lower pitching up moment. At the same time, the surface ratio between rudder and main foil amounts to 0.82 in order to strengthen the stability requirement. Furthermore, the value of the main foil's surface (0.1 m^2) comes from the trade-off between the stability and the efficiency and it guarantees the take-off condition at 3.5 m/s . Finally, if the stability is mainly influenced by the latter design variables, in order to enhance the efficiency of the configuration, the parameters to act on are the Aspect Ratios. It is understandable how their values lead to more efficient wing-foils because of the reduction of the induced drag component.

The preliminary design can be completed by evaluating the geometrical dimensions of foils. From the definition of the AR, the wing span and the mean aerodynamic chord are calculated. Furthermore, the root and tip chords are also obtained, by assuming a taper ratio ¹ of 0.6 [18].

$$AR = \frac{b^2}{S} = \frac{b}{\bar{c}} \quad (3.41)$$

$$c_{root} = \bar{c} \cdot \frac{3(1 + \lambda)}{2(1 + \lambda + \lambda^2)} \quad (3.42)$$

$$c_{tip} = c_{root}\lambda \quad (3.43)$$

From the **local optimization algorithm**, the equilibrium conditions are determined. Although they are representative of static conditions, they are also able to describe, with good approximation, the real operational behaviour of the boat. In fact, as the speed increases, the boat tends to rise up and stabilize the ride height at about 0.6 m. At the same time, in order to reduce the take off time, the pitch angle is positive resulting in a greater AoA of main foil i.e. greater lift. Moreover, the trend aims to reach and maintain an attitude as neutral as possible, by acting on the rudder foil control.

Finally, the design configuration guarantees both static and dynamic stability. The pitching moment derivative is negative, so that, after a disturbance causing an increase (or decrease) of the boat's attitude, the pitching moment is negative (or positive) allowing the boat to return to the equilibrium condition. In addition, the more the speed the more the stability due to the fact that drag components increase their influence. Looking at the dynamic behaviour, it is characterized by three real eigenvalues and one complex and conjugate pair leading to an oscillatory response.

$x_{mf}[m]$	$x_{rf}[m]$	$S_{mf}[m^2]$	$S_{rf}[m^2]$	$AR_{mf}[-]$	$AR_{rf}[-]$
1.53	3.79	0.1	0.082	10.92	8.67

Table 3.4: Results: Design variables

¹ λ = taper ratio in this context

$b_{mf}[m]$	\bar{c}_{mf}	$c_{root_{mf}}[m]$	$c_{tip_{mf}}[m]$	$b_{rf}[m]$	\bar{c}_{rf}	$c_{root_{rf}}[m]$	$c_{tip_{rf}}[m]$
1.04	0.095	0.016	0.07	0.84	0.097	0.018	0.071

Table 3.5: Results: main and rudder foil's geometry

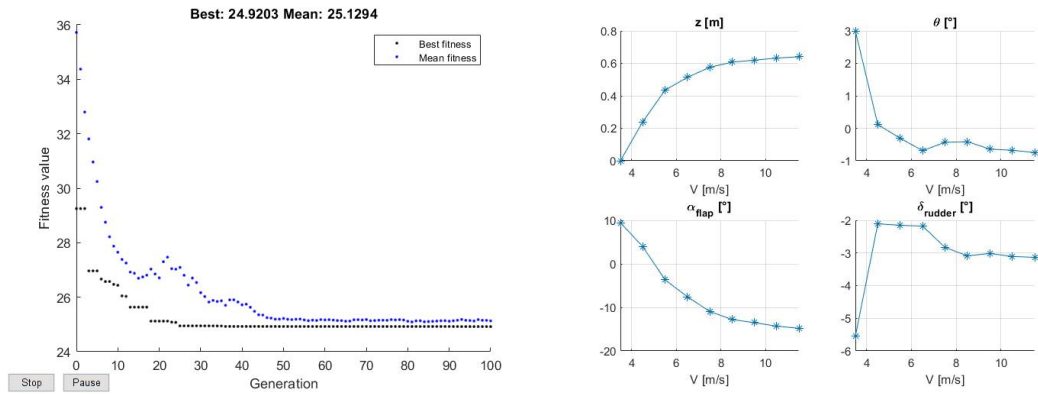


Figure 3.10: Results: GA iterations - equilibrium solutions

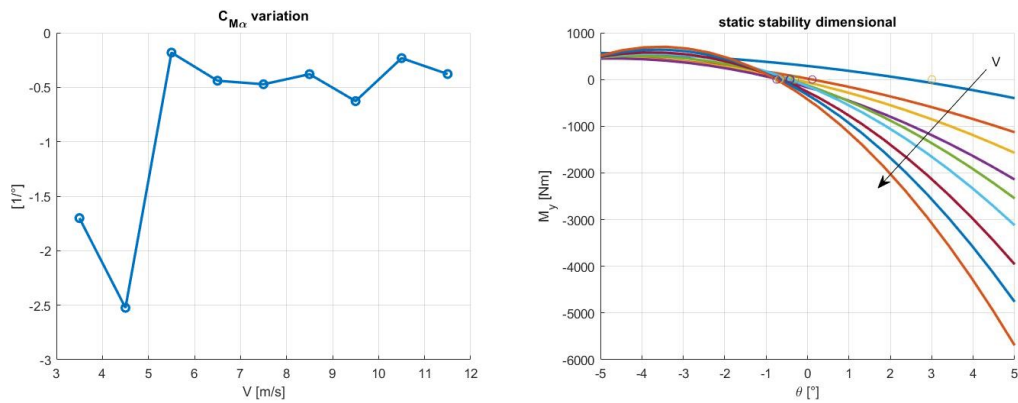
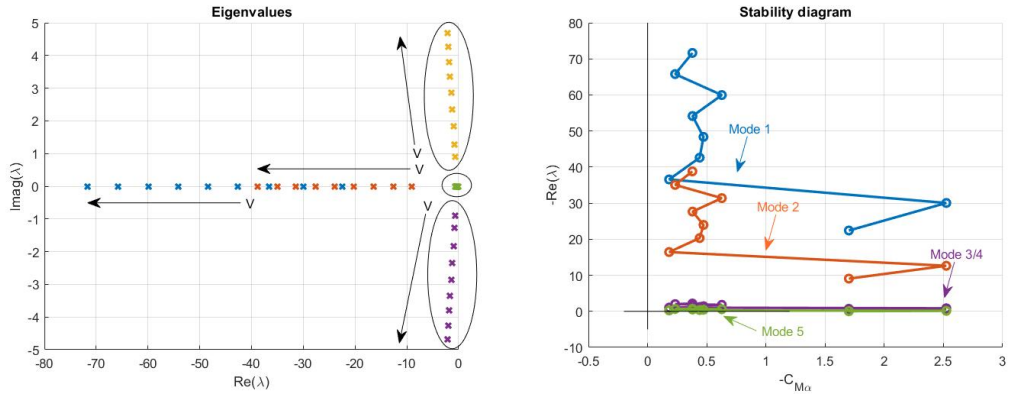


Figure 3.11: Results: static stability


Figure 3.12: Results: eigenvalues - stability diagram

$V[m/s]$	$\lambda_1[1/s]$	$\lambda_2[1/s]$	$\lambda_3[1/s]$	$\lambda_4[1/s]$	$\lambda_5[1/s]$
3.5	-22.403	-9.067	$-0.7063 + 0.896i$	$-0.7063 - 0.896i$	-0.046
4.5	-30.046	-12.634	$-0.843 + 1.278i$	$-0.843 - 1.278i$	-0.141
5.5	-36.565	-16.434	$-1.030 + 1.840i$	$-1.030 - 1.840i$	-0.264
6.5	-42.612	-20.313	$-1.206 + 2.347i$	$-1.206 - 2.347i$	-0.364
7.5	-48.360	-23.960	$-1.424 + 2.867i$	$-1.424 - 2.867i$	-0.445
8.5	54.145	-27.658	$-1.623 + 3.349i$	$-1.623 - 3.349i$	-0.518
9.5	59.961	-31.384	$-1.808 + 3.806i$	$-1.808 - 3.806i$	-0.586
10.5	65.770	-35.058	$-1.996 + 4.261i$	$-1.996 - 4.261i$	-0.652
11.5	71.637	-38.803	$-2.164 + 4.689i$	$-2.164 - 4.689i$	-0.718

Table 3.6: Results: modes

$V[m/s]$	$t_{1/2}(\lambda_1)[s]$	$t_{1/2}(\lambda_2)[s]$	$t_{1/2}(\lambda_3)[s]$	$t_{1/2}(\lambda_4)[s]$	$t_{1/2}(\lambda_5)[s]$
3.5	0.0309	0.0764	0.9813	0.9813	14.8805
4.5	0.0231	0.0549	0.8213	0.8213	4.9116
5.5	0.0190	0.0422	0.6725	0.6725	2.6185
6.5	0.0163	0.0341	0.5746	0.5746	1.9006
7.5	0.0143	0.0289	0.4868	0.4868	1.5542
8.5	0.0128	0.0251	0.4269	0.4269	1.3371
9.5	0.0116	0.0221	0.3834	0.3834	1.1810
10.5	0.0105	0.0198	0.3472	0.3472	1.0617
11.5	0.0097	0.0179	0.3203	0.3203	0.9645

Table 3.7: Results: decay time

Chapter 4

6 DOF dynamic model

The aim of this section is to provide an in deep description of the 6 DOF dynamic model, explaining assumptions and purposes for which the model could be used. After the introduction of reference systems, the focus moves on the physical model behind the foiling boats and finally a wide panoramic about the boat's controllers is presented.

4.1 Motivation and assumptions

Once the boat's configuration has been defined from the **optimization process**, the development of a dynamic model brings the design one step closer to the reality. In particular, the model aims to:

- Study the dynamic stability during all the regatta conditions;
- Perform real manoeuvres;
- Investigate the take off phase;
- Analyse the best possible setup for the flap control system and how it changes according to the different courses;
- Study the sailor-boat interaction;
- Provide information about most critical loads' conditions of the appendages.

It is important to underline that the model gives a global view of the boat-sailor system and does not focus on the fluid-dynamic and structural point of view. Therefore, phenomena like cavitation or fluid-structure interactions are not in the interest of this work.

The following assumptions underlie the formulation of the model:

- Fixed CoG position: considering a classic moth design with the most common sailor position at 2.8 m from the bow;
- Neglected the heel angle effect on the apparent wind calculation;
- The centre of effort of vertical appendages have the same longitudinal position as the corresponding foils;
- The centre of effort of vertical appendages in the centreline between foil and water surface;
- Fixed true wind direction, coming from the North.

4.2 Reference systems and model variables

The first step into the development of the model is the definition of the reference systems. In fact, their choice is crucial in order to explicit all variables involved and understand how they are connected with each other.

The origin lies on the centre of gravity placed at $\{x_g, y_g, z_g\} = \{2.12, 0, 0.755\}$ m from the bow and the deck plane. Moreover, axes orientation follows the aeronautic convection with the longitudinal axes towards the bow, and the vertical axes towards the water free surface:

- **BODY (B)** : follows the boat's movements. Dynamic equilibrium equations are written in this frame;
- **WATER (W)** : parallel with the water surface and oriented as the water speed (i.e. boat speed). This frame is useful to express lift and drag forces of foils and vertical appendages;
- **APPARENT WIND (AWA)** : parallel with the apparent wind, therefore aerodynamic sail's forces are decomposed into this frame;
- **INERTIAL (I)** : fixed frame, parallel to the water surface and having the longitudinal axes pointing to the North direction. Referring to this system, the boat's x, y positions, fly height and heading direction are identified.

From the top view, it is possible to describe:

- TWA: true wind angle between the TWS direction and the bow of the boat;
- V : boat's speed. Assuming no sea currents, it is the same as the incoming water stream;
- AWA: apparent wind angle between TWS and boat speed;

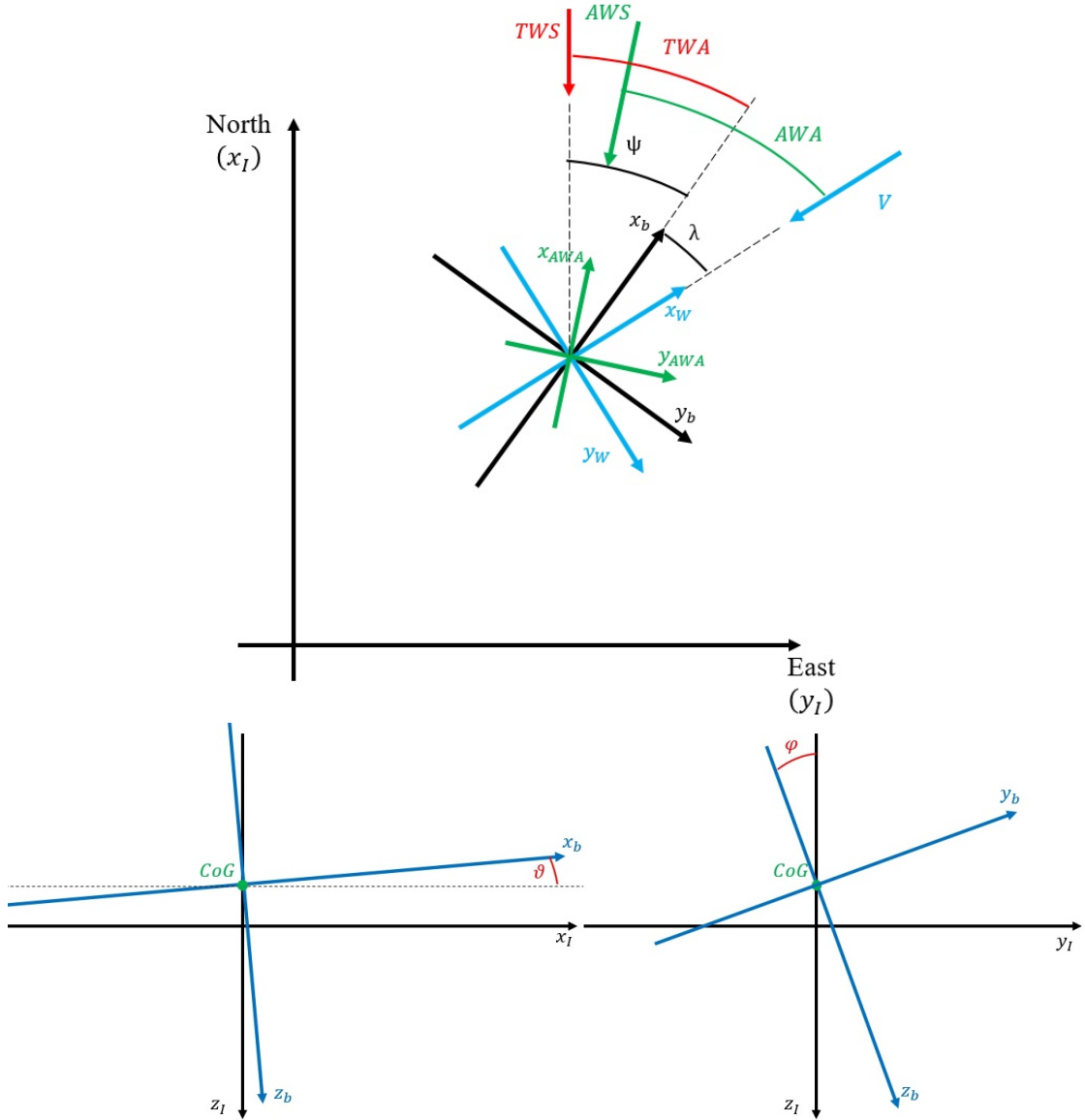


Figure 4.1: Reference frames 6 DOF: top,lateral,rear views

- λ : leeway angle between the longitudinal axes and the boat speed;
- Ψ : heading angle between longitudinal axes and North direction .

At this point, rotational matrixes are written to represent the linkage among reference frames. Therefore, following the forces' decomposition into the **W** and **AWA** frames, they are transferred to the **B** in order to write the equilibrium equations. More details are provided in the appendix A.1.

Further key steps in the development of the model consist on the identification of parameters representing the system's behaviour, the understanding of how the system is controlled and how it interacts with external forces. For this purposes, the following variables are declared:

- **Inputs:** represented by the true wind in both intensity TWS and direction TWA. As depicted in figure 4.1, it is chosen to represent the wind coming from the left side of the boat, thus with a negative sign. This will affect the apparent wind angle calculation as well as the apparent wind rotational matrix.
- **State variables:** necessary to describe the system:
 - u, v, w : boat's speed components into body axes;
 - p, q, r : speed angular rate around body axes;
 - ϕ, θ, ψ : Euler angles indicating the boat's attitude with the respect to the inertial frame;
 - x_I, y_I, z_I : boat's position into inertial axes.

$$\bar{x} = \{u, v, w, p, q, r, \psi, \theta, \phi, x_I, y_I, z_I\}^T \quad (4.1)$$

- **Control variables:** necessary to control the boat evolution:
 - α_{flap} : main foil flap angle, regulating the amount of lift generated by the main foil;
 - δ_r : rudder foil angle, regulating the attitude of the boat;
 - γ_r : rudder angle, regulating the direction of the boat;
 - x_{sailor}, y_{sailor} : longitudinal and lateral sailor position;
 - p : power of the sail, regulating the amount of total sail force and moment generated.

	velocity [m/s]	position [m]	angle [deg]	angular rate [1/deg]
X	u (surge)	x	ϕ (roll or pitch)	p (roll)
Y	v (sway)	y	θ (pitch)	q (pitch)
Z	w (heave)	z (ride height)	ψ (heading)	r (yaw)

Table 4.1: State variables

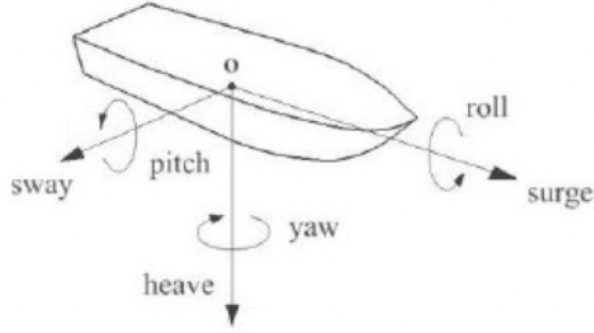


Figure 4.2: DOF names

4.3 Force modules

The effectiveness of the entire model depends on the accuracy of the description of the several physical phenomena involved. Since the hydrofoiling boats are complex systems, being composed of different elements strongly interacting with each other, distinguish their peculiarities became crucial for a successful outcome.

4.3.1 Foils

By generating lift to fly over the water surface, foils represent the cutting edge in the world of sailing. In order to underline their main contributions to the dynamic performance and to avoid a computationally-heavy model, the foil's forces formulation is based on the classic lift and drag expressions. However, in accordance with the pre-described static model (section 3.2), typical phenomena such as the free surface or the wave drag effect are included, as well as dynamic aspects.

Particular emphasis will be placed on the lift and drag coefficients. It is well-known how they mainly depends on the hydro-dynamic characteristics of profile and on the direction of the incoming water flow:

$$\begin{aligned}
 C_L &= C_{L\alpha_{3D}} \cdot \alpha \\
 C_D &= C_{D_0} + \frac{C_L^2}{e\pi AR} + C_{D_{wv}} = C_{D_0} + \frac{C_{L\alpha_{3D}}^2}{e\pi AR} \cdot \alpha^2 + C_{D_{wv}}
 \end{aligned}
 \tag{4.2}$$

Furthermore, the angle of attack depends on the attitude of the boat, the setting angles and the control variables:

$$\begin{aligned}
 \alpha_{mf} &= \alpha_g + i_{mf} + \tau \cdot \alpha_{flap} \\
 \alpha_{rf} &= \alpha_g + i_{rf} + \delta_r
 \end{aligned}
 \tag{4.3}$$

However, as the dynamic movements occur, the water direction changes, causing

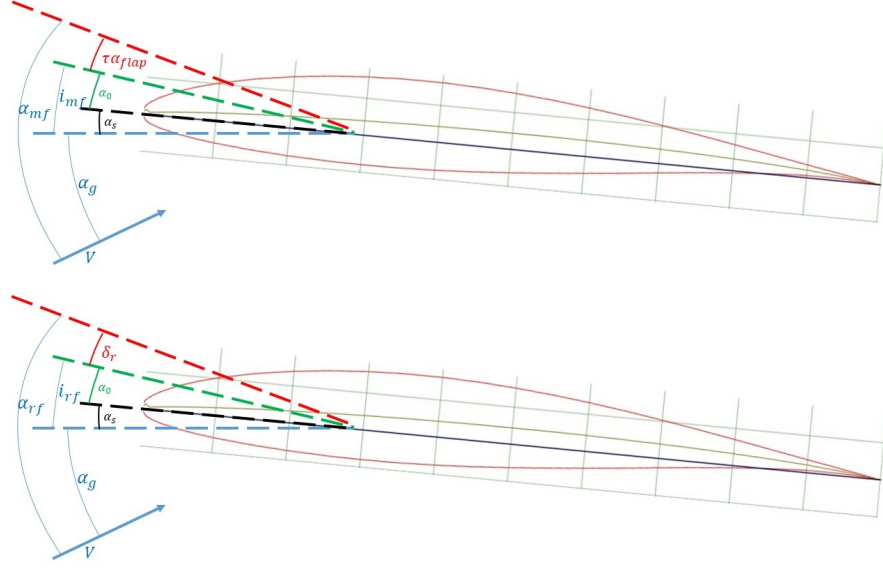


Figure 4.3: Main and rudder foil aerodynamic angles

a deviation from the static value of the angle of attack. These terms lead to the “*lifting damping effect*” because they bring the hydrodynamic surfaces to reduce the forces’ magnitude as the boat is moving.

- **Vertical speed w** : as the boat goes up ($w < 0$), the foil is affected by a reduction of the angle of attack due to the combination between horizontal and vertical speed:

$$\Delta\alpha_{mf_w} = \Delta\alpha_{rf_w} = \arctan\left(\frac{w}{u}\right) \quad (4.4)$$

- **Pitch rate q** : as the boat tends to pitch up ($q > 0$), a vertical speed variation of the two foils occurs. In particular, the main foil is affected by a reduction of the angle of attack while the one of the rudder foil increases its value:

$$\begin{aligned} \Delta\alpha_{mf_q} &= -\arctan\left(\frac{q(x_g - x_{mf})}{u}\right) \\ \Delta\alpha_{rf_q} &= \arctan\left(\frac{q(x_{rf} - x_g)}{u}\right) \end{aligned} \quad (4.5)$$

By resuming, the total expression of the angle of attack is:

$$\begin{aligned} \alpha_{mf} &= \alpha_g + i_{mf} + \tau\alpha_{flap} + \Delta\alpha_{mf_w} + \Delta\alpha_{mf_q} \\ \alpha_{rf} &= \alpha_g + i_{rf} + \delta_r + \Delta\alpha_{rf_w} + \Delta\alpha_{rf_q} \end{aligned} \quad (4.6)$$

4.3.2 Vertical appendages

Daggerboard and rudder guarantee the lateral and direction control of the boat. In fact, their hydro-dynamic forces, generated by the leeway angle λ , act in the opposite direction of the sail, preventing the boat from losing its desired course. If the lateral control is intrinsic on the system, the rudder γ_R guarantees the directional control, i.e. the heading control.

Moreover, while foils' platform is constantly immersed, the vertical appendages' wetted surface changes with the fly height, resulting in a consequent variation of forces and moments. In particular, as the height increases, the wetted surface is reduced and the centre of pressure moves downwards, causing shift away from the centre of gravity. Assuming that the centre of pressure is placed in the centreline between the foil and the water surface, the relationships among submerged length, fly height and pitch angle can be stated:

$$\begin{aligned} l_D &= L_D - z_I - \theta(x_g - x_{mf}) \\ l_R &= L_R - z_I + \theta(x_{rf} - x_g) \end{aligned} \quad (4.7)$$

$$\begin{aligned} S_D &= c_D L_D \\ S_R &= c_R L_R \end{aligned} \quad (4.8)$$

$$\begin{aligned} z_D &= \frac{l_D}{2} + z_I + h_{hull} + z_g \\ z_R &= \frac{l_R}{2} + z_I + h_{hull} + z_g \end{aligned} \quad (4.9)$$

It is worth noticing that l_D and l_R must be considered inside the free surface and wave drag corrections of foils, since they represent their current distance from the water. Moreover, the latter equations are valid in flying conditions, so when z_I has a positive value. Finally, the *Aspect Ratio* is affected too, causing a small variation into the induced drag component as well as in the lift curve slope:

$$\begin{aligned} AR_D &= \frac{l_D}{c_D} \\ AR_R &= \frac{l_R}{c_R} \end{aligned} \quad (4.10)$$

Similarly to foils, the boat movement leads to change the angle of attack of the vertical appendages too. In particular:

- **Leeway angle** λ : it takes into account both static and dynamic effects due to the lateral speed v . It is defined by:

$$\lambda = \arctan\left(\frac{v}{V}\right) \quad (4.11)$$

- **Yaw rate** r : as the boat is rotating around the z_b axes, the resulting angle of attack variation is:

$$\begin{aligned} \Delta\alpha_{D_r} &= \arctan\left(\frac{r(x_g - x_{mf})}{u}\right) \\ \Delta\alpha_{R_r} &= -\arctan\left(\frac{r(x_{rf} - x_g)}{u}\right) \end{aligned} \quad (4.12)$$

- **Roll rate** p : as the boat is rotating around the x_b axes, the resulting angle of attack variation is:

$$\begin{aligned} \Delta\alpha_{D_p} &= -\arctan\left(\frac{pz_D}{u}\right) \\ \Delta\alpha_{R_p} &= -\arctan\left(\frac{pz_R}{u}\right) \end{aligned} \quad (4.13)$$

By resuming, the total expression of the angle of attack is:

$$\begin{aligned} \alpha_D &= \lambda + \Delta\alpha_{D_r} + \Delta\alpha_{D_p} \\ \alpha_R &= \lambda + \gamma_r + \Delta\alpha_{R_r} + \Delta\alpha_{R_p} \end{aligned} \quad (4.14)$$

Because of hydro-dynamic forces are developed in the $x_b - y_b$ plane, vertical appendages are not affected by the free surface or wave drag corrections, so lift and drag coefficient are simply given by:

$$\begin{aligned} C_L &= C_{L\alpha_{3D}} \alpha \\ C_D &= C_{D_0} + \frac{C_L^2}{e\pi AR} \end{aligned} \quad (4.15)$$

4.3.3 Hull

The buoyancy force is the one who models the hull. With the assumption of considering the hull shape as rectangular, it is possible to express the submerged volume as the product between the platform area and the submerged length:

$$F_{buoyancy} = \rho g (S_{hull} \cdot l_{hull}) \quad (4.16)$$

Obviously, this force is active only if the fly height is less than the buoyancy height, assumed half the hull height.

4.3.4 Sail

Sail represents the core element providing the driving force. However, it is the most complex at the same time, being the primary means of interaction between boat and sailor. In fact, in addition to forward movement, sail's force is responsible of the lateral motion and the capsizing moment. Consequently, through the numerous adjustments, the helmsman must be able to find a balance between the desire to go faster and maintain a stable equilibrium condition. More details about this control are described in the following sections 4.5.

As far as sail model is concerned, it involves a huge effort with CFD methods, or real measurements. In this thesis, the work of Boegle [4] is taken into account. By neglecting the effect of the heel angle on the apparent wind direction, sail's lift and drag coefficients are expressed as function of the AWA with an interpolation of the original data. This results in the following.

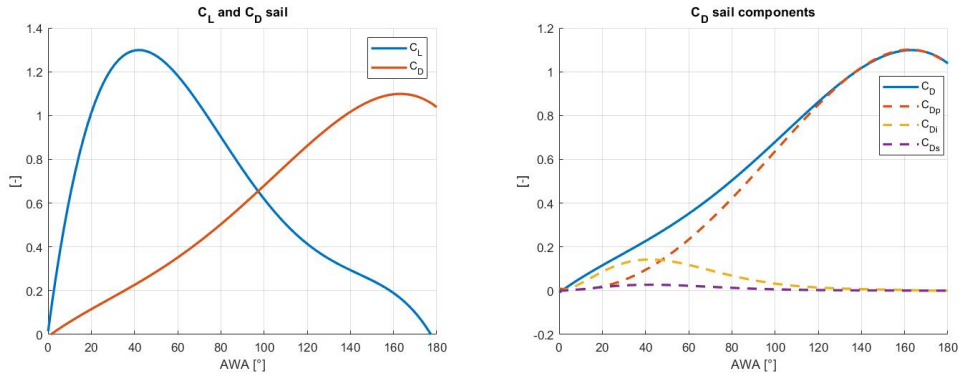


Figure 4.4: Sail polars

The sail drag coefficient takes into account:

- **Separation drag** C_{D_s} obtained with the product between lift coefficient and drag separation constant $C_{D_s} = C_L^2 c_s$;
- **Induced drag** C_{D_i} defined as $C_{D_i} = \frac{C_L^2}{e\pi AR}$;
- **Parasitic drag** C_{D_p} that is the dominant effect.

4.4 Equilibrium equations

The equilibrium of the system is based on the *D'Alembert principle* [14] stating that the sum of external and inertial forces and moments is zero:

$$\begin{aligned} \vec{F}_{ext} - \frac{d\vec{Q}}{dt} &= 0 \\ \vec{M}_{ext} - \frac{d\vec{K}}{dt} &= 0 \end{aligned} \quad (4.17)$$

By going through the expression, momentum and angular momentum derivatives can be made explicit into the body frame:

$$\begin{aligned} \frac{d\vec{Q}}{dt} &= \dot{Q}_x \vec{i} + \dot{Q}_y \vec{j} + \dot{Q}_z \vec{k} + Q_x \frac{d\vec{i}}{dt} + Q_y \frac{d\vec{j}}{dt} + Q_z \frac{d\vec{k}}{dt} = \dot{\vec{Q}} + \vec{\omega} \times \vec{Q} \\ \frac{d\vec{K}}{dt} &= \dot{K}_x \vec{i} + \dot{K}_y \vec{j} + \dot{K}_z \vec{k} + K_x \frac{d\vec{i}}{dt} + K_y \frac{d\vec{j}}{dt} + K_z \frac{d\vec{k}}{dt} = \dot{\vec{K}} + \vec{\omega} \times \vec{K} \end{aligned} \quad (4.18)$$

Furthermore, considering the \vec{Q} , \vec{K} and $\vec{\omega}$ definition gives:

$$\begin{aligned} \vec{\omega} &= p\vec{i} + q\vec{j} + r\vec{k} \\ \vec{Q} &= mu\vec{i} + mv\vec{j} + mw\vec{k} \\ \vec{K} &= K_x\vec{i} + K_y\vec{j} + K_z\vec{k} = \\ &= (pI_x - rI_{xz} - qI_{xy})\vec{i} + (qI_y - rI_{yz} - pI_{xy})\vec{j} + (rI_z - pI_{xz} - qI_{xy})\vec{k} \end{aligned} \quad (4.19)$$

$$\begin{aligned} \vec{\omega} \times \vec{Q} &= \begin{vmatrix} \vec{i} & \vec{j} & \vec{k} \\ p & q & r \\ mu & mv & mw \end{vmatrix} = [m(qw - rv)]\vec{i} + [m(ru - pw)]\vec{j} + [m(pv - qu)]\vec{k} \\ \vec{\omega} \times \vec{K} &= \begin{vmatrix} \vec{i} & \vec{j} & \vec{k} \\ p & q & r \\ K_x & K_y & K_z \end{vmatrix} = (qK_z - rK_y)\vec{i} + (rK_x - pK_z)\vec{j} + (pK_y - qK_x)\vec{k} \end{aligned} \quad (4.20)$$

The only null cross product inertia is the I_{xy} . In fact, in spite of the boat symmetry, the sailor contribution gives rise to I_{yz} term. Finally, the general set of dynamic equation is stated:

$$\begin{cases} F_x = m(\dot{u} + qw - rv) \\ F_y = m(\dot{v} + ru - pw) \\ F_z = m(\dot{w} + pv - qu) \\ M_x = I_x \dot{p} + (I_z - I_y)qr - I_{xz}(\dot{r} + pq) - I_{yz}(q^2 - r^2) \\ M_y = I_y \dot{q} + (I_x - I_z)rp - I_{xz}(p^2 - r^2) - I_{yz}(\dot{r} - pq) \\ M_z = I_z \dot{r} + (I_y - I_x)pq - I_{xz}(\dot{p} - rq) - I_{yz}(q^2 - r^2) \end{cases} \quad (4.21)$$

As far as external forces are concerned, they come from the force modules previously expressed with the addition of the sailor's weight and position. In particular, forces and moments developed by the boat elements are enclosed together as an algebraic sum, while the sailor's forces and moments are considered separately:

$$\begin{aligned} X, Y, Z &= \sum_{i=1}^6 R_{i_b}(1,2,3) \\ L, M, N &= \sum_{i=1}^6 M_{i_b}(1,2,3) \end{aligned} \quad (4.22)$$

Where:

- X, Y, Z : resulting body forces along x_b, y_b, z_b axes respectively;
- L, M, N : resulting body moments around x_b, y_b, z_b axes respectively;
- R_{i_b} : resulting force of the i - element into body axes;
- M_{i_b} : resulting moment of the i - element into body axes;

Finally, adding the external forces and moments due to boat and sailor weight, the dynamic equations are obtained. Moreover, kinematic equations are necessary in order to complete the set of equations:

$$\begin{cases} F_x = m(\dot{u} + qw - rv) = X - W \sin(\theta) \\ F_y = m(\dot{v} + ru - pw) = Y + W \cos(\theta) \sin(\phi) \\ F_z = m(\dot{w} + pv - qu) = Z + W \cos(\theta) \cos(\theta) \\ M_x = I_x \dot{p} + (I_z - I_y)qr - I_{xz}(\dot{r} + pq) - I_{yz}(q^2 - r^2) = L - W_{sailor} y_{sailor} \cos \phi \\ M_y = I_y \dot{q} + (I_x - I_z)rp - I_{xz}(p^2 - r^2) - I_{yz}(\dot{r} - pq) = M + W_{sailor} x_{sailor} \cos \theta \\ M_z = I_z \dot{r} + (I_y - I_x)pq - I_{xz}(\dot{p} - rq) - I_{yz}(q^2 - r^2) = N \end{cases} \quad (4.23)$$

$$\begin{cases} \dot{\phi} = p + q \sin(\phi) \tan(\theta) + r \cos(\phi) \tan(\theta) \\ \dot{\theta} = q \cos(\phi) - r \sin(\phi) \\ \dot{\psi} = q \frac{\sin(\phi)}{\cos(\theta)} + r \frac{\cos(\phi)}{\cos(\theta)} \end{cases} \quad (4.24)$$

$$\begin{cases} \dot{x}_I = u \cos(\theta) \cos(\psi) + v(-\cos(\phi) \sin(\psi) + \sin(\phi) \sin(\theta) \cos(\psi)) + \\ w(\sin(\phi) \sin(\psi) + \cos(\phi) \sin(\theta) \cos(\psi)) \\ \dot{y}_I = u \cos(\theta) \sin(\psi) + v(-\cos(\phi) \cos(\psi) + \sin(\phi) \sin(\theta) \sin(\psi)) + \\ w(-\sin(\phi) \sin(\psi) + \cos(\phi) \sin(\theta) \sin(\psi)) \\ \dot{z}_I = u \sin(\theta) - v \sin(\phi) \cos(\theta) - w \cos(\phi) \cos(\theta) \end{cases} \quad (4.25)$$

It is important to highlight that:

- m is the total mass given by the sum of boat and sailor mass;
- W is the total weight given by the sum of boat and sailor weight;
- x_{sailor} and y_{sailor} represent the sailor's distance from the *CoG* of the system. They are considered with positive values;
- Inertia terms take into account the boat and the sailor inertia (appendix A.2);
- The last equation represents the vertical speed with an opposite sign with respect of the vertical inertial axes. This way, as the boat goes up, the vertical speed is positive as well as the vertical position. Moreover, it is worth to remember that:
 - $z_I < 0$ in the displacement condition;
 - $z_I = 0$ when the hull base is touching the water;
 - $z_I > 0$ when the boat is flying.

4.5 Controllers

This section aims to provide a broad understanding of the main controllers required to handle an *International Moth*. Their use is fundamental to ensuring stable dynamic behaviour and achieving the desired sailing conditions. It should be emphasised how the helmsman is the principal governor of the craft by acting on all systems, from the sail, to the rudder, to the main foil. However, the latter is fully automatic and adjustments are sporadic and aimed at changing trim conditions. Therefore, for the modelling purposes, for the main foil control system only well-defined equations can be written, while the others simulate the sailor's behaviour, and the theory of P-I-D controllers [19] is involved.

4.5.1 Main foil control system

The main foil control system is the crucial component of a *Moth* being capable of guarantee a stable flight. Following the introduction on the main elements composing the system in 2.3, the performance are now analysed. The input comes from the wand sensor, located at the bow and constantly in contact with the water. Therefore, α_{wand} is strictly related to the fly height and, being jointed to the boat, depends on its attitude too [5].

$$\alpha_{wand} = \begin{cases} \arccos\left(\frac{z_I}{|\cos\phi|l_{wand}}\right) - \theta & \frac{z_I}{|\cos\phi|} < l_{wand} \\ 0 & \frac{z_I}{|\cos\phi|} \geq l_{wand} \end{cases} \quad (4.26)$$

On the buoyancy regime, the fly height is less than zero and the wand angle is at the maximum value represented by the ratio between the waterline height and the length of the wand. As the boat is flying higher, the wand rotates towards the bow thus reducing the wand angle.

The bow mechanism converts the wand rotation into a horizontal movement of the push rod and the downstream kinematics leads to the deflection of flap. After the analysis of all variables involved (details in A.3), the correlation between flap angle and ride height is obtained for both systems: **Mach2** and **BugsCam**. The

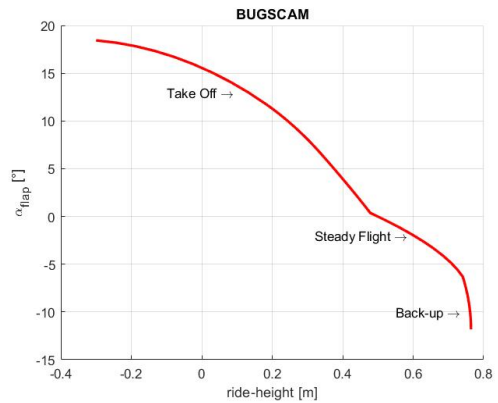
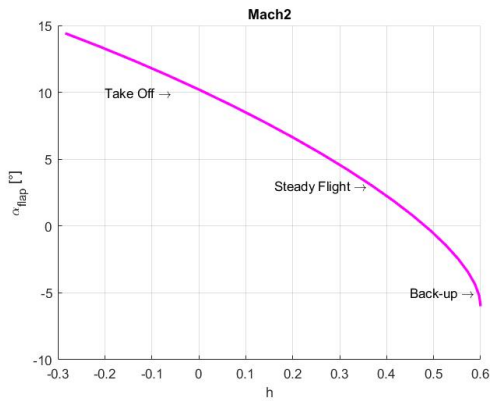


Figure 4.5: Mach2: performance curve **Figure 4.6:** BugsCam: performance curve

two performance curves shows the same trend of the flap angle. However, the **BugsCam** presents a marked difference among the various flight stages, while the sensitivity of the **Mach2** is almost constant apart from the “Back-up” zone where, even a small height variation leads to a wider flap movement.

4.5.2 Rudder foil control system

While the main foil control system is involved into the ride height control, the rudder foil is **sailor-managed** via a screw nut mechanism in order to control the pitching attitude of the boat. In fact, by changing the rudder foil angle of attack, more pitching up/down moment is generated because of the rear lift variation. In contrast to the main foil, in this case, the overall rudder is movable with an external joint structure placed at the stern of the hull called “*gantry*”. The longitudinal sailor’s movements could also control the pitching angle, but usually, the sailing style suggests to stand still and operates with the tiller of the rudder. Nevertheless, when a massive pitch angle variation is required, the only rudder action is not sufficient and the movement is inevitable.

As far as cruise phase is concerned, the desired pitch angle depends on the performance and on the sailor's preferences. In particular, with the *AC-75*, the American's Cup boats, the most efficient trim consists of a small pitch down angle, but for an *International Moth* there is no a great difference. For this reason, the desired θ is set at 0° in order to have a flat boat and easy to prevent nosedive into water. On the other hand, during the take off phase, sailor can pitch up the boat and take advantage of the greater main foil angle of attack to reduce the take off time and space.

P-I-D controller is implemented for both the rudder foil and longitudinal sailor position, by imposing saturation values due to the mechanism's movement limits, airfoil inefficiency and sailor movement limits.

4.5.3 Rudder directional control system

It represents the directional control allowing the boat to follow a desired path and change course direction. Good rudder control leads to a great manoeuvrability in racing scenarios where the boat must change wind direction frequently, especially in the upwind conditions. The P-I-D law is implemented, with heading ψ as controlled variable and rudder angle γ_r as control variable.

With the assumption that the true wind direction is coincident with North, the TWA is the equivalent of the heading and vice versa.

Therefore, at the beginning of the simulation the wind orientation, and consequently the heading angle, is fixed in order to investigate an upwind or downwind take-off phase. However, to perform manoeuvres, the desired ψ is modified and the wind conditions change automatically:

$$\begin{cases} \text{if } t = 0 & \psi_0 = |TWA| \\ \text{else} & TWA = |\psi| \end{cases} \quad (4.27)$$

4.5.4 Roll motion control

As stated by all the moth sailors, controlling the roll motion is the most critical part of sailing a moth. In fact, they spend most of their time managing this equilibrium to avoid catastrophic consequences. In order to have a high fidelity model of the roll motion control, it is necessary to study in depth the sailor's behaviour and how forces are generated by the other elements of the boat.

As explained in the previous sections, the sail provides the driving force to move forward, but, because of the apparent wind direction, a lateral force component is generated. Daggerboard and rudder aims to contrast the latter to prevent the path lose and thus guarantee the F_y equilibrium. However, from a rear view, it is possible to understand how the equilibrium moment around the longitudinal

axes M_x is not satisfied and the sailor must intervene to contrast this **capsizing moment**. To mitigate the latter, the typical moth sailing style consists on flying with an upwind heel angle. In addition, having a heel angle allows the boat to reduce the leeway angle, and thus the drag of the vertical appendages.

From these lines, the complexity of the problem is evident, due to the numerous couplings between the equations. In spite of this, the two most important variables on which to act are the sailor lateral position y_{sailor} and sail power p . Assuming an optimum heel angle of $\phi_{des} = -15^\circ$, leading to an upwind condition, the real behaviour is based on the following ideas:

- $\phi < \phi_{des}$: it means that the boat is too much heeled upwind. To reach the desired condition, the system has to generate a positive roll moment. To do so, it is necessary to give maximum power to the sail and move the sailor towards the centre of the boat;
- $\phi > \phi_{des}$: it means that the boat is with a more downwind heel angle than the desired condition. In order not to lose sail power, and therefore speed, the first reaction is the helmsman's movement towards the outer position while the sail is still fully powered;
- $\phi \gg \phi_{des}$: it means that the boat is too much rolled downwind. The sailor's weight is not enough to achieve the desired heel angle and a depowering of the sail depower is necessary.

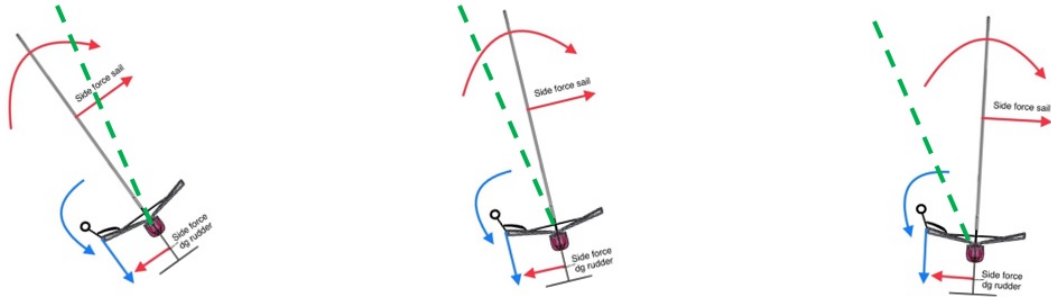


Figure 4.7: Roll motion control

The model stems from these ideas and takes the Heggert thesis work as reference [5]. In particular, the two control variables are combined into one called M_{xctr} , to reflect the sequence of sailor movements and sail depower. As already mentioned, the priority is to maintain the sail's power as long as possible to exploit the driving force. Once the sailor's weight cannot longer ensure the balance, the sail must be

depowered.

For this reason, M_{xctr} ranges from 0 to 1.8:

- Range 0 – 1 represents the condition in which sailor is moving, while sail is totally powered:

$$\begin{cases} y_{sailor} = M_{xctr} \cdot y_{sailor_{max}} \\ p = 1 \end{cases} \quad (4.28)$$

- Range 1 – 1.8 represents the condition in which sailor is placed at the maximum outer position and sail is depowered:

$$\begin{cases} y_{sailor} = y_{sailor_{max}} \\ p = 2 - M_{xctr} \end{cases} \quad (4.29)$$

For example, if $M_{xctr} = 1.2$ it means $y_{sailor} = y_{sailor_{max}}$ and $p = 0.8$.

As done for the other controls, a P-I-D controller is used, with ϕ as controlled variable and M_{xctr} as control variable.

The parameter *power* has a direct effect on the lift and drag coefficient as well as on the centre of effort of the sail. In this context, the work of Hansen [20] is taken as reference to describe the sail depowering model. Even though this model does not represent the physical change of the sail geometry given by the different adjustments available, it gives a wider view of the effects in the generation of forces and moments.

Power is defined as the ratio between the actual heeling moment coefficient and the optimum heeling moment coefficient representing fully powered sail:

$$p = \frac{C_{M_x}}{C_{M_{x_{opt}}}} \quad (4.30)$$

Therefore, by different measurements it is possible to find regression parameters to connect C_L , C_D , z_{sail} and power p :

$$\begin{aligned} C_L &= C_{L_{opt}} \cdot p^{a_1} \\ C_D &= C_{D_s} + C_{D_i} + C_{D_p} = c_s C_L^2 p^{a_5} + \frac{C_L^2}{e\pi AR} p^{a_6} + C_{D_{opt}} (a_3 + (1 - a_3)p^{a_4}) \\ z_{sail} &= z_{sail_{opt}} \cdot p^{a_2} \end{aligned} \quad (4.31)$$

a_1	a_2	a_3	a_4	a_5	a_6
0.7	0.3	0.42	1.82	3.21	-1.1

Table 4.2: Regression parameters

4.6 Simulation results

In this section the main results are presented with the aim to describe the physical coherence of the model and provide a comparison between different wind conditions. Simulations are carried out with the boat's configuration given by the **optimization tool** and with the **BugsCam** as main foil control system.

The simulation conditions are summarized as follows:

- $TWS = 5 \frac{m}{s}$;
- $TWA = -50^\circ$;
- $\bar{x}_0 = \{u_0, v_0, w_0, p_0, q_0, r_0, \phi_0, \theta_0, \psi_0, x_0, y_0, z_0\} = \{1.5, 0, 0, 0, 0, 0, 0, 0, 50^\circ, 0, 0, 0\}$

At the beginning of the simulation, the boat is in the bouancy regime and the hull force is the dominat effect.

At the same time, the sail driving force leads to an increase of the logitudinal speed u and, as a consequence, the lift forces became sufficient to bring the boat away from the free surface. In fact, after 3.76 s the nullyfing of the hull force occurs, which means that the craft is no longer in contact with the water.

Meanwhile, the boat tends to move towards $\phi_{des} = -15^\circ$. This leads to significant fluctuations in sail force due to the continuous power/de-power, needed to balance the rolling moment, as well as the variation of AWA and AWS as the boat's speed increases. Nevertheless, the coupoling with the lateral equilibrium causes leeway angle oscillations that are reflected in the daggerboard and rudder forces. At the same time, the longitudinal attitude is also involved due to the sail pitching down effect.

Finally, when the rolling motion is expired, the sail force assumes an almost constant value, and the equilibrium of the system is thus guaranteed.

As far as take-off performance are concerned, the boat configuration is capable of lift off from the water after 3.76 s when the speed reaches 3.8 m/s. This feature is in accordance with the optimization tool assumption of take-off speed equal to 3.5 m/s. However, this slight difference is attributed to the static approximations such as neglecting the hull resistance and the sail force variations.

Moreover, the **BugsCam** control system provides 15° of flap at take-off, resulting in **zone 1** of the curve. As the height increases, the flap angle drops down until

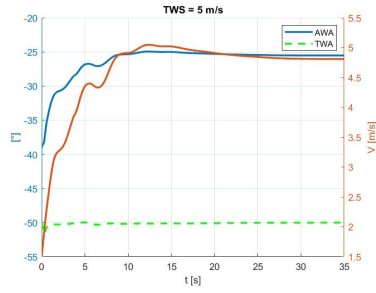


Figure 4.8: Results: TWS = 5 m/s TWA = 50°: AWA variation

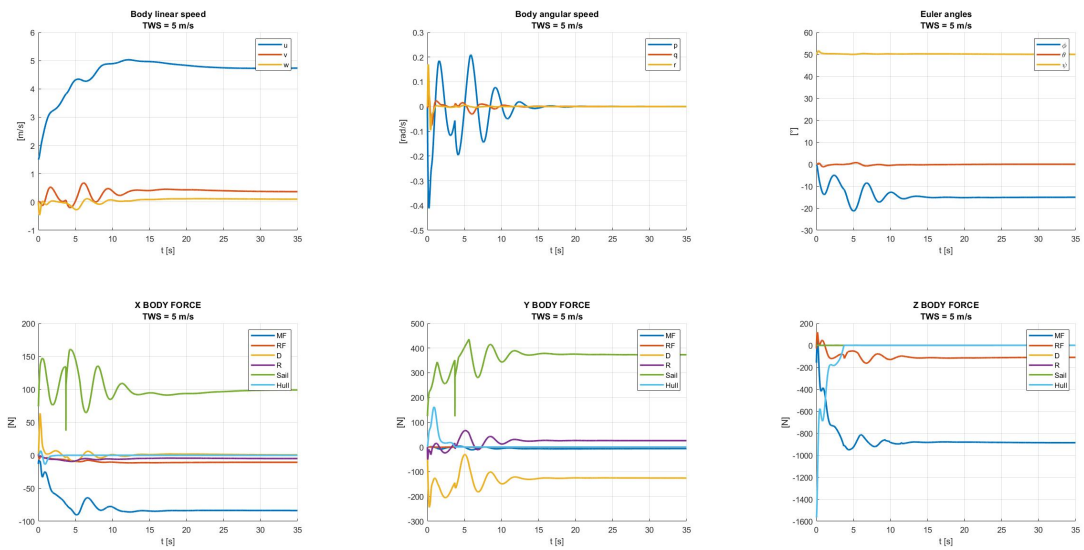


Figure 4.9: Results TWS = 5 m/s TWA = 50°: speeds, body forces

reaching a regime condition at about 0° in the **zone 3**, corresponding with a steady flight at $0.63 m$.

Investigating the longitudinal motion, the pitch angle is subjected to high frequency oscillations with an amplitude less than 2° . As a results of the P-I-D controller, the rudder foil control system is stressed by continuous adjustments. The take-off phase is characterized by a slight pitch up attitude in order to increase the AoA of the main foil.

The majority of θ fluctuations are caused by the roll motion control, acting of the sail force. In particular, at the beginning of the simulation the helmsman is in the outer position and the sail is depowered. After a few seconds, the situation reverses and, when the sail power is maximum, the pitch angle drops to a negative value. Finally, at the end of the continuous sail adjustments, the desired heel angle

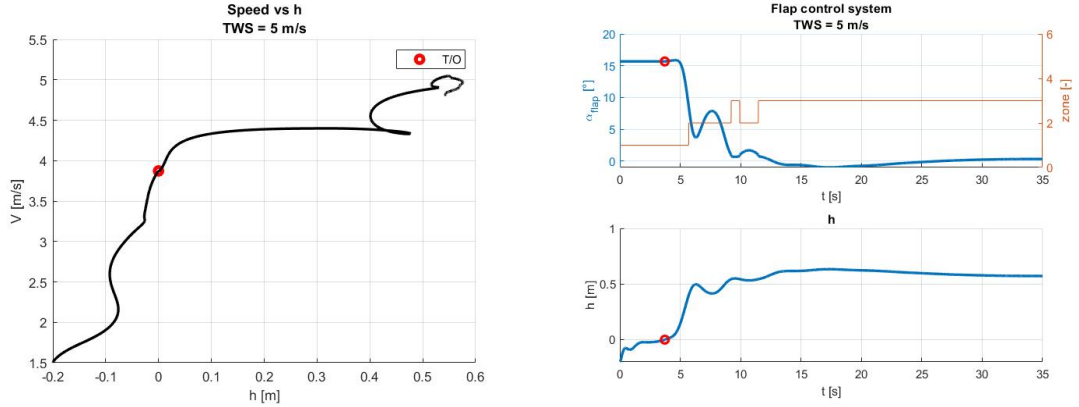


Figure 4.10: Results $TWS = 5 \text{ m/s}$ $TWA = 50^\circ$: TO speed, control system

is reached in less than 15 seconds and the steady sail power is 0.7.

At the same time, the flight height is influenced by the two variables θ and ϕ , because their effects are strictly related to the lift force distribution. In fact, a change in the pitch angle results in a variation in foils angles of attack, while sail power/de-power leads to a different boat speed. The directional control is guaranteed with a positive rotation of the rudder angle around the z_b axes.

With the same initial conditions and $TWA = -50^\circ$, a further simulation is carried out to investigate the effect of the true wind intensity. It is assumed a true wind speed of 8 m/s .

First, the resulting AWA and AWS are increased and, thus, the sail force is enhanced. Therefore, the take off time falls down to 2.44 s . The boat's speed reaches a maximum of about 6 m/s resulting in a higher flight condition. Consequently, the control system regime zone is the fourth, the most sensitive.

However, despite more wind speed, the boat speed tends to assume the same steady-state value of the former condition. The main reason is that the rolling moment equilibrium is guaranteed by a sail power of 0.35 (about half of the previous simulation) and less oscillations occur. In fact, even small adjustments are amplified by the increased strength of the sail. Finally, as far as pitch moment equilibrium is concerned, the rudder foil equilibrium is achieved at about -4.5° in order to provide a more intensive pitching up moment and, thus, counteract the pitching down effect of sail.

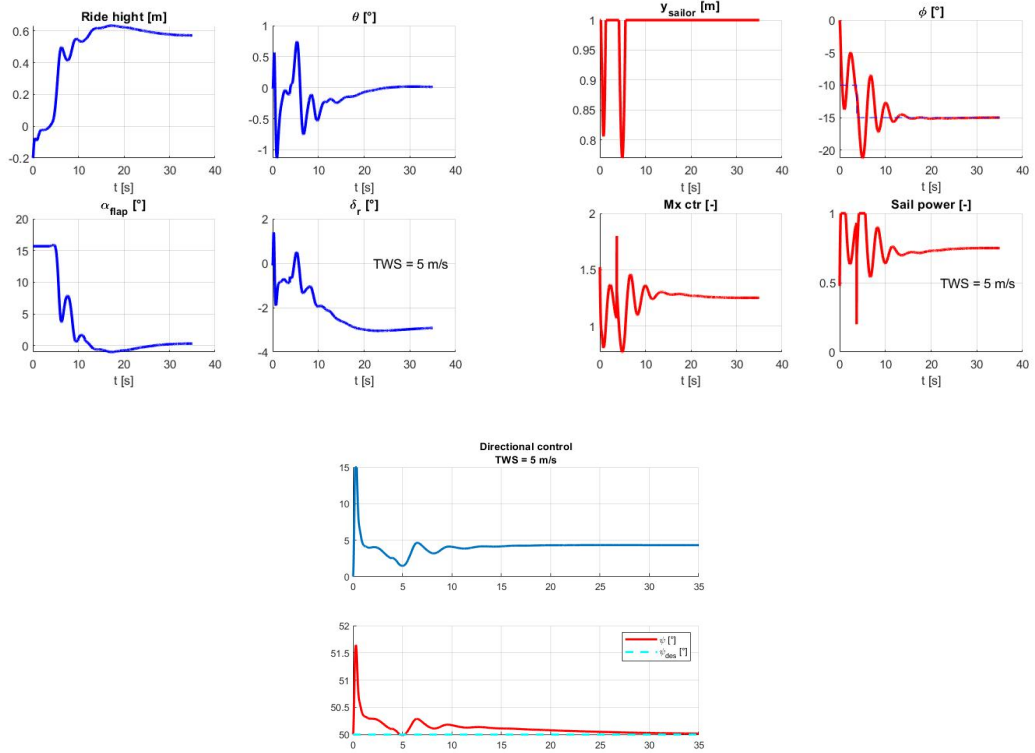


Figure 4.11: Results TWS = 5 m/s TWA = 50°: longitudinal,roll motion,directional controls

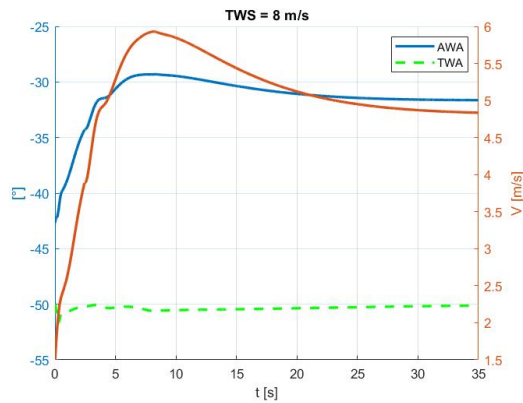


Figure 4.12: Results: TWS = 8 m/s TWA = 50°: AWA variation

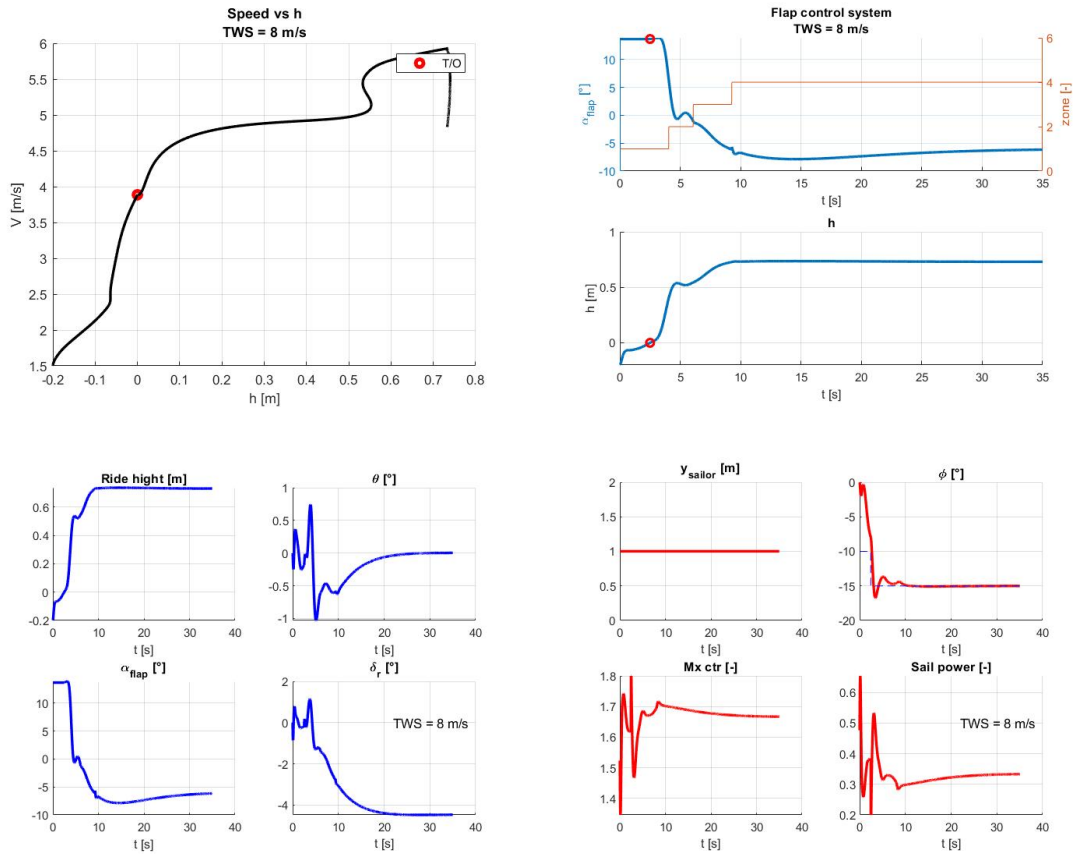


Figure 4.13: Results TWS = 8 m/s TWA = 50°: TO, flap, longitudinal, roll motion

Chapter 5

Stability assessments

From the previous sections 3.4, the linearized model was described to investigate the boat's stability through the small perturbation theory. It is a useful tool in the first stages of design. However, downstream the development of the 6 DOF dynamic model, further details can be added and the linear model can be validated. In doing so, it is important to highlight the fact that only the longitudinal motion is taken into account. Moreover, the linearized model does not include the boat's controllers, apart from the main foil control system. Therefore, to have a real comparison between the linear and non-linear response, it is necessary to adapt the 6 DOF model.

At first, the complete dynamic simulation is performed, by inputting the TWS and TWA conditions. Once the regime is achieved, the equilibrium points are saved. At this stage, a disturbance on the state variables is introduced. Simultaneously, the three degree of freedom outside the longitudinal plane are frozen ($F_y = M_x = M_z = 0$) and the controllers are disabled. Thereby, the non-linear and controlled 6 DOF model is converted into a non-linear 3 DOF with the only main foil control system as active controller.

In the following simulations, $TWS = 8 \text{ m/s}$ and $TWA = 50^\circ$ are considered and a disturbance of 0.15 m in the fly height is given.

The eigenvalues shows a stable dynamic behaviour, in accordance with the expectations. In particular, the response is dominated by an oscillatory mode, with a damping factor of $\zeta = 0.38$ and a natural frequency of $\omega_n = 4.54 \text{ rad/s}$, and an aperiodic mode with a decay time $t_{1/2} = 1 \text{ s}$.

By comparing the linear and non-linear responses, it is noticeable a similar trend of the state variables. In fact, a drop in fly height is followed by an increase of drag, and therefore the speed is reduced. In addition, the free surface effect is less influent and the lift coefficients are risen up, resulting in an ascent speed ($w < 0$) and a pitching up moment ($q, \theta > 0$). However, the non-linear response is affected

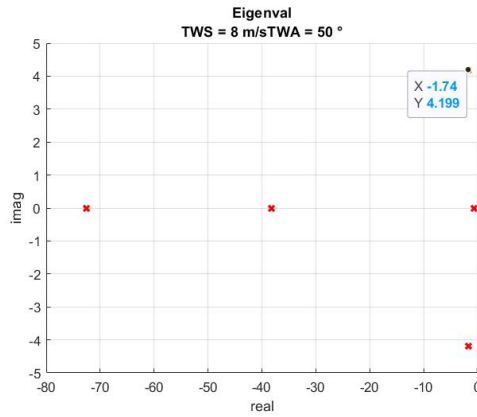


Figure 5.1: TWS = 8 m/s TWA = 50° : Eigenvalues

by more oscillations than the linear one. This could be attributable to the linear model neglecting the sail force variation as function of the AWA and AWS, as stated by [15]. Nevertheless, the eigenmodes are run out in fifteen seconds without the helmsman’s action.

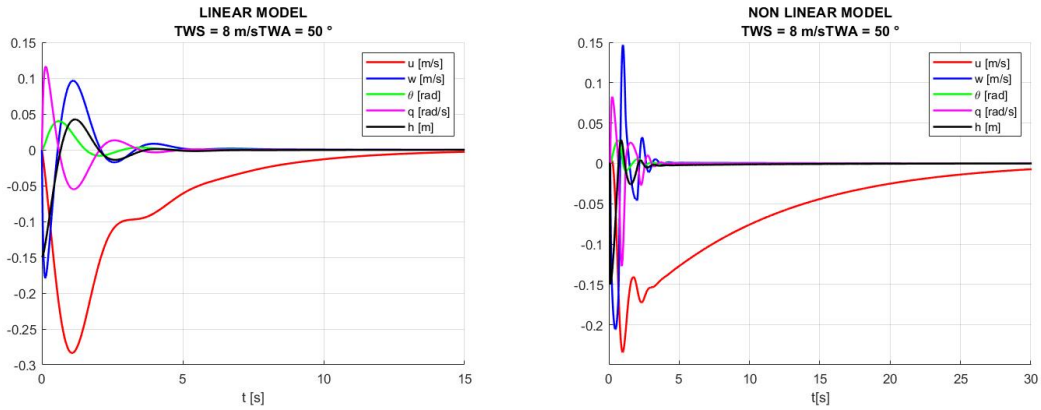


Figure 5.2: Linear and Non-linear response ($\Delta h = 0.15m$)

An in deep investigation, regarding the contribution of **main foil control system** to the stability is provided.

From the mathematical point of view, the control system affects the variation of flap angle as function of the ride height, thus introducing the derivative $\frac{\delta\alpha_{flap}}{\delta h}$. It influences the main foil’s lift coefficient resulting in a different boat’s dynamic response.

By taking into account the same wind conditions of the previous simulation, it is clear that the control system leads to a more damped and faster response (figure

5.4). In fact, the derivative $C_{L_{h_{mf}}}$ decreases by two order of magnitude, if a constant flap angle is considered. Therefore, the variation of lift forces is only based on the free surface effect.

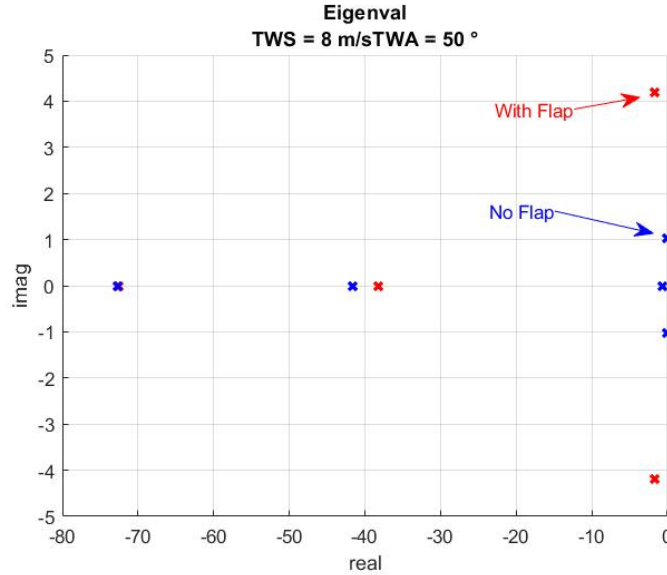


Figure 5.3: Flap effect: Eigenval

$\zeta_{withflap}$	ζ_{noflap}	$\omega_{n_{withflap}} [\frac{rad}{s}]$	$\omega_{n_{noflap}} [\frac{rad}{s}]$	$C_{L_{h_{mf}}_{withflap}} [\frac{1}{m}]$	$C_{L_{h_{mf}}_{noflap}} [\frac{1}{m}]$
0.38	0.03	4.54	1.05	2.13	0.0937

Table 5.1: Dynamic response characteristics

Finally, a comparison between the performance of **Mach2** and **BugsCam** is presented. In particular, the investigation concerns the systems' capability to prevent the boat from jumping out of the water. Therefore, simulations are carried out with the same wind conditions and an impulsive disturbance (tab ??) on the ride height is introduced, once the regime condition is achieved.

Following an increase of the fly height, the **BugsCam** system immediately switches to the “**back-up**” zone providing a huge and rapid variation of the flap angle. As a consequence, the boat tends to go down and the operating zone is restored to the **third** one (regime condition). After four seconds, the pulse signal drops to zero, causing a downward disturbance for the system. Therefore, the **zone 2** is activated and the flap angle assumes a positive value to provide a greater amount of lift. This would lead to a significant height increase. However, the **zone 4** brings the boat back to the equilibrium condition. It is worthy of highlight the asymmetry in

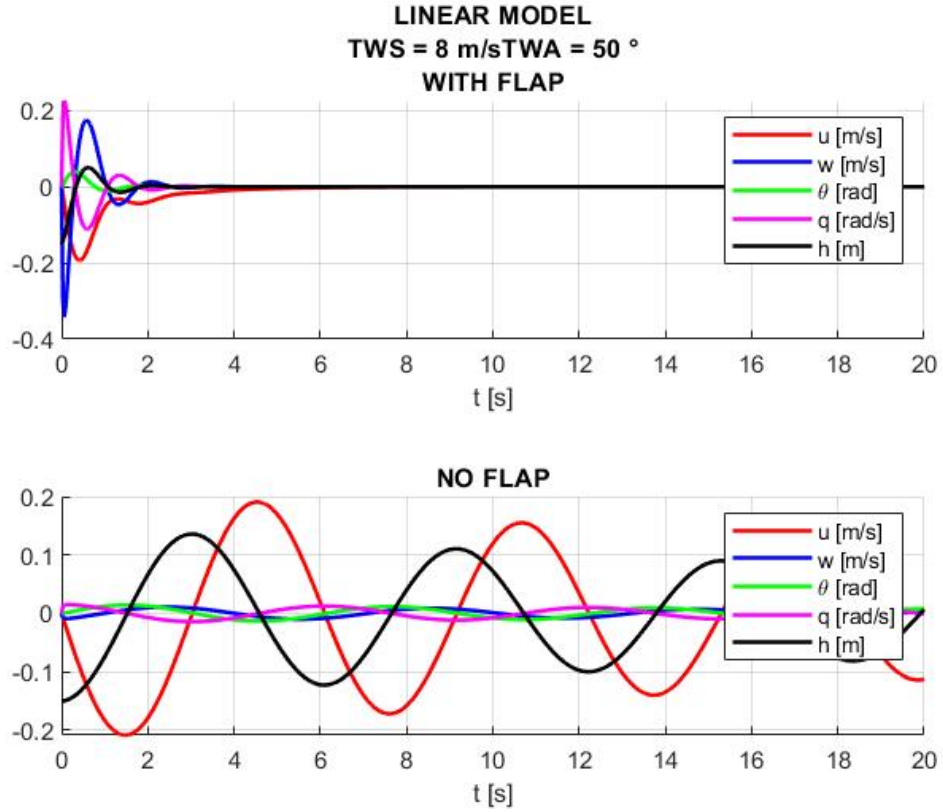


Figure 5.4: Flap effect: time response

Period [s]	Pulse Width [%]	Amplitude [m]	Delay [s]
20	5	0.15	40

Table 5.2: Impulsive disturbance

the intervention of zone 4 and 2. In fact, this latter is the zone characterized by the greatest sensitivity, resulting in a strong effect on flap angle and its effect is limited for a small range of α_{wand} .

On the contrary, since the **Mach2** does not have a severe “back-up” zone, it controls the boat with a smoother behaviour and avoids the flap from high-demanding variations.

Furthermore, in order to simulate the wave motion, a sinusoidal disturbance is analysed. It can be observed how the **BugsCam** tends to cut the upper peaks due to the continuous transitions between the regime and the “back-up” zone. Nevertheless, in the **Mach2** system this effect is not evident.

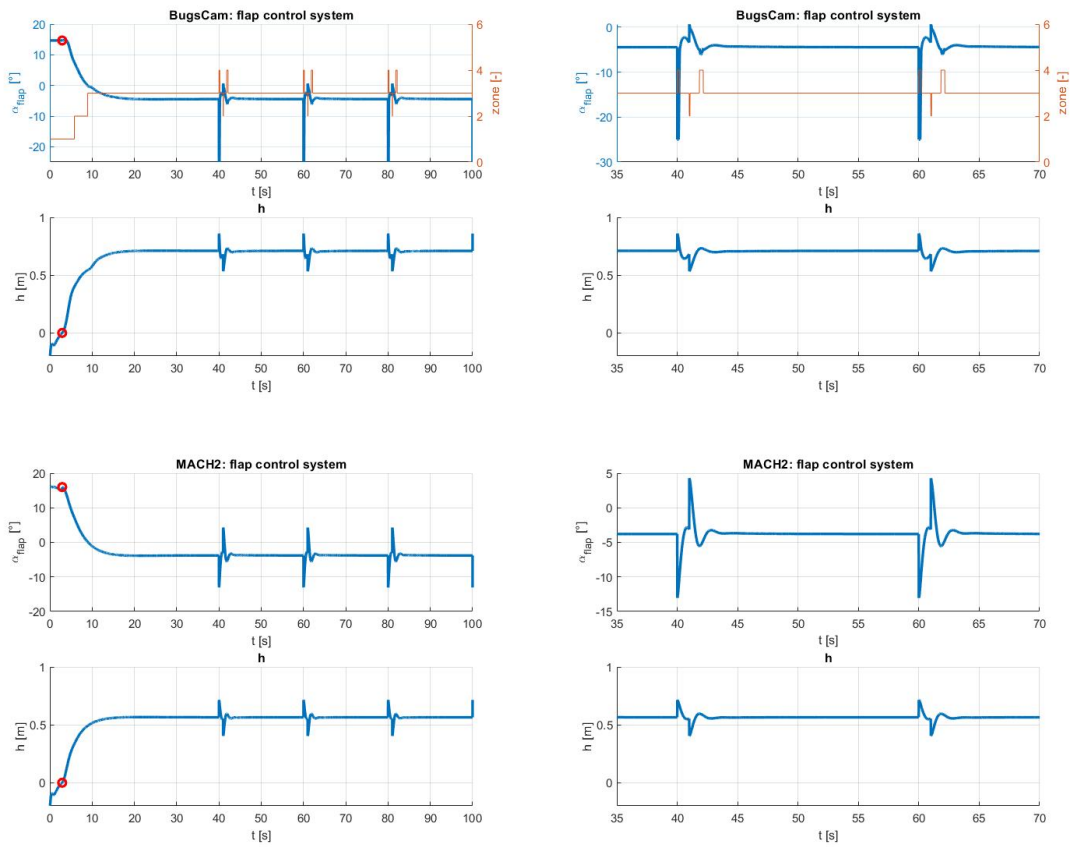


Figure 5.5: Response to impulsive disturbance $\Delta h = 0.15m$

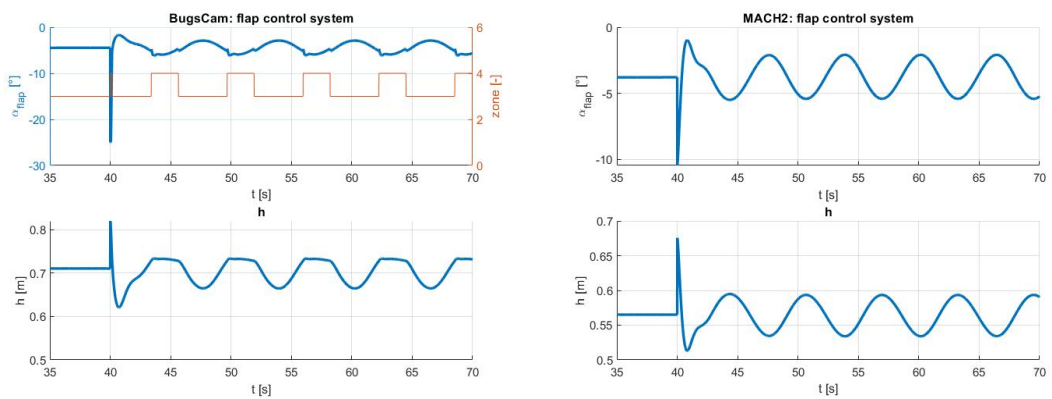


Figure 5.6: Response to sinusoidal disturbance

Chapter 6

Maneuvers

One of the main reasons behind the development of the **6 DOF dynamic model**, was the possibility to carry out maneuvers simulations. This could allow both designers and sailors to test the boat's performance or predict the sailor-boat interactions that will occur during the regatta.

In the following the **Bearing away** maneuver is simulated (figure 6.1). Therefore, the boat aims to change the course direction with respect to the North. On doing so, the action of the rudder controller is essential in order to create the necessary yawing moment and change the bow's orientation. As a consequence, the true wind condition is different and so does the apparent wind. This leads to a lower sail's side-force and results in a less heeled attitude. The following steps are, thus,

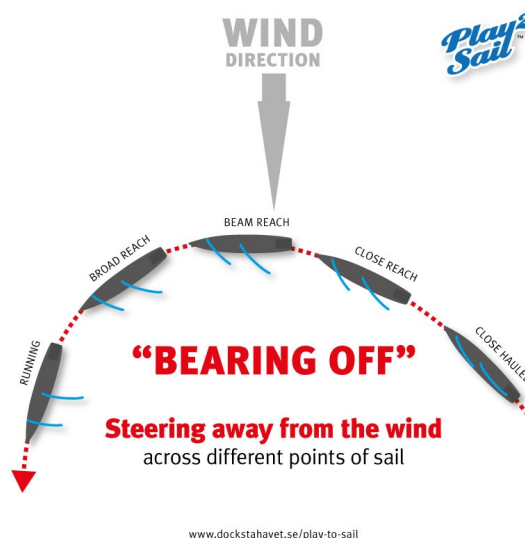


Figure 6.1: Bearing Away maneuver [21]

performed to set up the simulation:

1. $TWS = 5 \text{ m/s}$;
2. $TWA = -50^\circ$;
3. Initial conditions: $\bar{x}_0 = \{u_0, v_0, w_0, p_0, q_0, r_0, \phi_0, \theta_0, \psi_0, x_0, y_0, z_0\} = \{1.5, 0, 0, 0, 0, 0, 0, 0, 0, -TWA, 0, 0, 0\}$;
4. At 50s the desired heading is switched, through a ramp signal with a rate of $10^\circ/s$;
5. At 50s the desired heel angle is switched from $\phi_{des} = -15^\circ$ to $\phi_{des} = -8^\circ$.
At the same time, the P-I-D gains, controlling the roll motion, are adapted to the new condition.

The first noteworthy result concerns the boat speed. In accordance with reality, when sailing downwind, the speed increases beyond the TWS. This is due to the change in the apparent wind, which results in a more powerful sail (i.e. a higher driving force) and at the same time a lower lateral force. Therefore, with a true wind speed of 5 m/s , the boat's speed goes from about 4.8 m/s in upwind, to about 6.8 m/s in downwind course. As a result, the main foil produces more lift, which leads to a significant increase in sailing height, and, without acting on the control system settings, the **BugsCam**'s operating zone goes from third to fourth. In fact, it is a common practice to shorten the transmission rod, by acting on the **offset**, to reduce the flap angle.

Meanwhile, during the change of course, the optimum heel angle is reduced and the

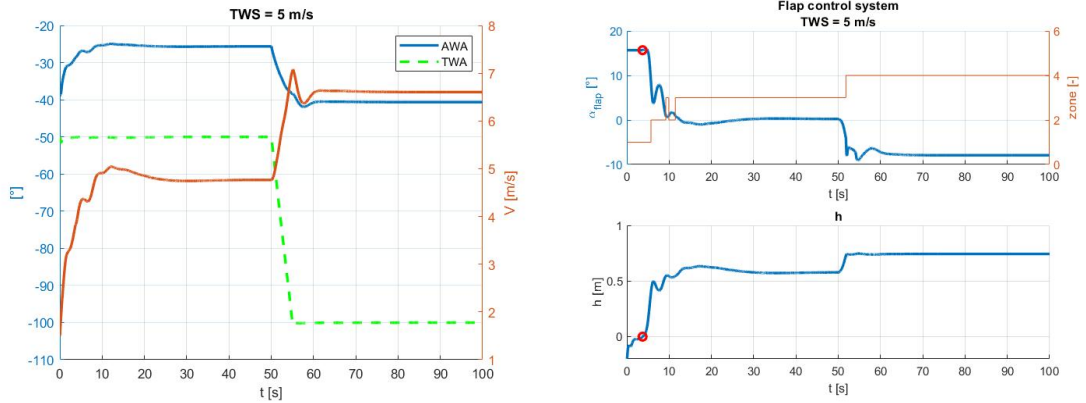


Figure 6.2: Maneuver: AWA variation, BugsCam control system

sailor must move towards the centre of the boat first and then manage sail power.

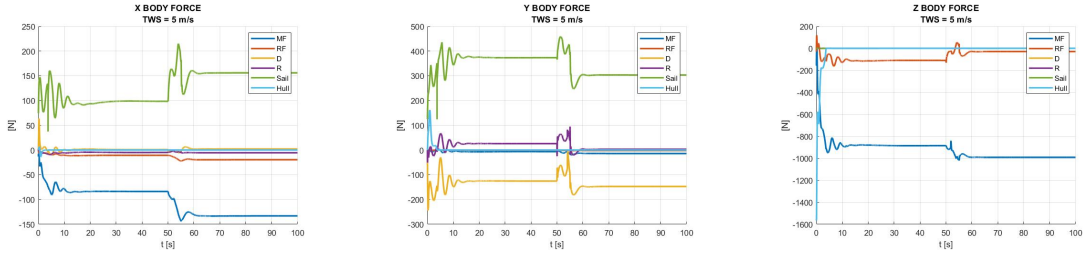


Figure 6.3: Maneuver: X,Y,Z body forces

The regime value of sail power is similar for upwind and downwind conditions, however, as already described, it refers to two different magnitudes of sail force. As far as pitching attitude is concerned, it remains approximately constant, with some slight fluctuations ($< 0.5^\circ$).

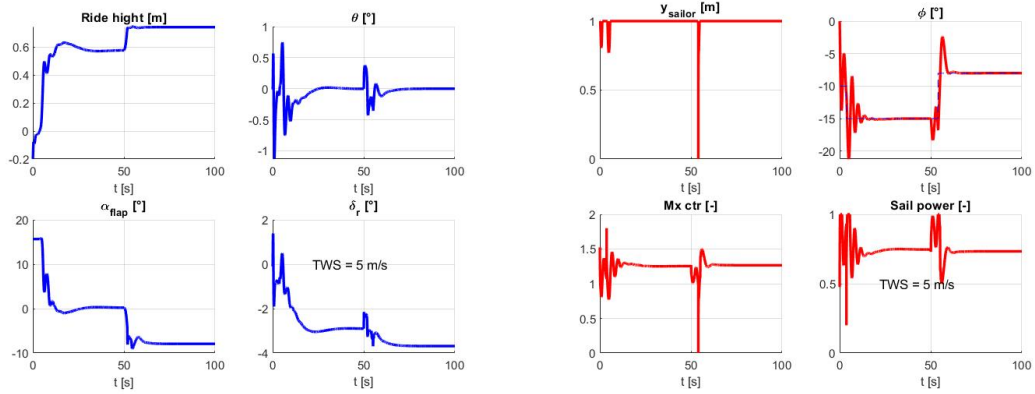


Figure 6.4: Maneuver: Longitudinal, Roll motion control

Finally, a 3D representation of the maneuver is provided. Following the take-off phase, the boat heads towards North-East, while after fifty seconds orientation is towards South-East. The differences between the real and the desired path are due to the leeway angle. This deviation is reduce in downwind because of the decrease of sail's lateral force component.

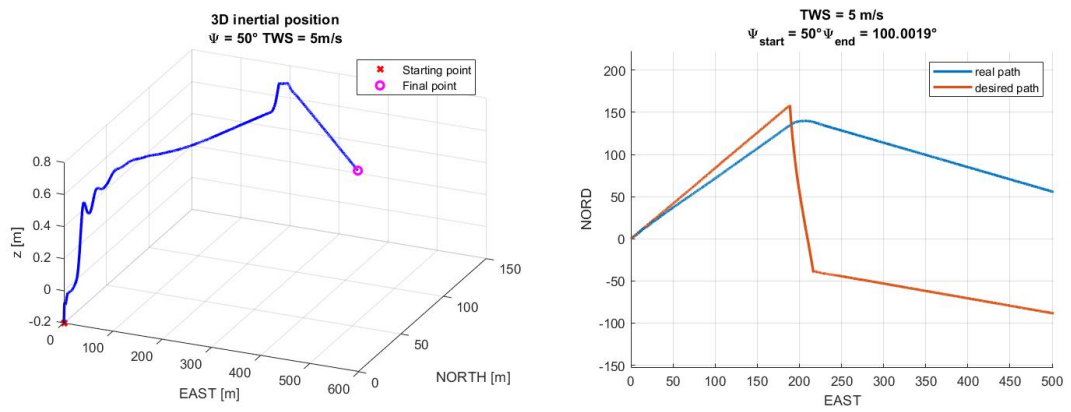


Figure 6.5: Maneuver: 3D path

Chapter 7

Conclusion and future work

This thesis work, starting from the definition of the high-level requirements for an *International Moth*, was capable of designing an optimum configuration, by means of an **optimization tool** and to simulate its performance through the development of a **6 DOF dynamic model**.

In particular, the implementation of a **genetic algorithm** made it possible to compare the numerous possible designs and select the most suitable one to comply with stability and efficiency requirements. For this purpose, a 2 DOF static model and a linearized model were developed. Through them, a **local algorithm** evaluated the trim conditions and the performance parameters.

Once the boat's configuration was defined, it was simulated in order to investigate dynamic performance and carry out regatta-like manoeuvres. The **6 DOF dynamic model** was based on simple assumptions and the formulation took its cue from flight mechanics theory. Nevertheless, all relevant aspects of the boat's dynamic behaviour were taken into account. In particular, considerable emphasis was placed on the **sailor-boat** interactions by modelling all the on-board controls and adjustments. Furthermore, an in deep analysis of the **main foil control system** was carried out. The **Mach2** and the **BugsCam** system were compared and the importance of the system in ensuring the stability of the boat was proved. Finally, the **bearing away** manoeuvre was simulated and a good correlation was observed between the simulated results and the expected real behaviour.

Some of the possible work improvements are resumed below.

As far as the **optimization tool** is concerned, it can be enhanced by taking into account the wind effect. Therefore, the would pass from 2 DOF to 3 DOF where the boat's speed is a new state variable. This way, the resultant boat's configuration would be the optimum one for the regatta field.

Furthermore, in order to have a more detailed description of the boat's system,

foil's setting angles (i_{mf}, i_{rf}) or foil's sweep angles $(\Lambda_{mf}, \Lambda_{rf})$ should be added. The approximation of assuming the same airfoil, can be overcome by considering NACA profile parameters within the optimization. However, the expression of forces and aerodynamic coefficients would require a more detailed definition. Alternatively, the tool should provide an external link with software analysis such as X-FOIL [22].

Improvements on the **6 DOF dynamic model** could concern the control laws and the take-off phase analysis.

In particular, it would be possible to exploit the linearized model to incorporate controllers such as LQR [23] or H_∞ [24], thus expanding the applicability of the model to more comprehensive wind conditions. Moreover, the main foil control system adjustments (offset and gearing) should be included, in order to have a more detailed sailor-boat interaction model.

Finally, a more thorough formulation of the hull's forces and moments would lead to a better understanding of the water-air transition.

Appendix A

Appendix

A.1 Forces components

As stated in previous chapters (4.2) **WATER** and **APPARENT WIND** reference systems are used to express lift and drag forces of each element. To write them, the following consideration must be taken into account:

- Drag forces are in the opposite direction of the longitudinal axes x_b because they are developed along speed direction;
- Lift forces of main foil and rudder foil are in the opposite direction of the vertical axes z_b ;
- Lift and drag forces of daggerboard and rudder depends on their angles of attack (α_D, α_R);
- Lift and drag forces of sail depends on the AWA;
- Hull force aligned with vertical inertial axes z_I .

$$\begin{aligned} R_{mfW} &= \begin{Bmatrix} -D_{mf} \\ 0 \\ -L_{mf} \end{Bmatrix} R_{rfW} = \begin{Bmatrix} -D_{rf} \\ 0 \\ -L_{rf} \end{Bmatrix} \\ R_{DW} &= \begin{Bmatrix} -D_D \\ -\text{sign}(\alpha_D)|L_D| \\ 0 \end{Bmatrix} R_{RW} = \begin{Bmatrix} -D_R \\ -\text{sign}(\alpha_R)|L_R| \\ 0 \end{Bmatrix} \\ R_{sailAWA} &= \begin{Bmatrix} -D_{sail} \\ -\text{sign}(AWA)|L_{sail}| \\ 0 \end{Bmatrix} R_{hull_I} = \begin{Bmatrix} 0 \\ 0 \\ -F_{hull} \end{Bmatrix} \end{aligned} \quad (\text{A.1})$$

Furthermore, matrix representing the rotation around one single axes are:

$$\begin{aligned}
 \Psi &= \begin{bmatrix} \cos(\psi) & -\sin(\psi) & 0 \\ \sin(\psi) & \cos(\psi) & 0 \\ 0 & 0 & 1 \end{bmatrix} \\
 \Theta &= \begin{bmatrix} \cos(\theta) & 0 & \sin(\theta) \\ 0 & 1 & 0 \\ -\sin(\theta) & 0 & \cos(\theta) \end{bmatrix} \\
 \Phi &= \begin{bmatrix} 1 & 0 & 0 \\ 0 & \cos(\phi) & -\sin(\phi) \\ 0 & \sin(\phi) & \cos(\phi) \end{bmatrix} \\
 AWA &= \begin{bmatrix} \cos(AWA) & -\sin(AWA) & 0 \\ \sin(AWA) & \cos(AWA) & 0 \\ 0 & 0 & 1 \end{bmatrix} \\
 \Lambda &= \begin{bmatrix} \cos(\lambda) & -\sin(\lambda) & 0 \\ \sin(\lambda) & \cos(\lambda) & 0 \\ 0 & 0 & 1 \end{bmatrix} \\
 \alpha_D &= \begin{bmatrix} \cos(\alpha_D) & -\sin(\alpha_D) & 0 \\ \sin(\alpha_D) & \cos(\alpha_D) & 0 \\ 0 & 0 & 1 \end{bmatrix} \\
 \alpha_R &= \begin{bmatrix} \cos(\alpha_R) & -\sin(\alpha_R) & 0 \\ \sin(\alpha_R) & \cos(\alpha_R) & 0 \\ 0 & 0 & 1 \end{bmatrix}
 \end{aligned} \tag{A.2}$$

Then, in order to express forces into body axes, rotational matrices are stated (subscripts represent final and starting reference frame respectively).

$$\begin{aligned}
 L_{BW} &= [\Lambda][\Theta] = \begin{bmatrix} \cos(\lambda) & -\sin(\lambda) & 0 \\ \sin(\lambda) & \cos(\lambda) & 0 \\ 0 & 0 & 1 \end{bmatrix} \begin{bmatrix} \cos(\theta) & 0 & \sin(\theta) \\ 0 & 1 & 0 \\ -\sin(\theta) & 0 & \cos(\theta) \end{bmatrix} \\
 L_{BAWA} &= [AWA][\Theta] = \begin{bmatrix} \cos(AWA) & -\sin(AWA) & 0 \\ \sin(AWA) & \cos(AWA) & 0 \\ 0 & 0 & 1 \end{bmatrix} \begin{bmatrix} \cos(\theta) & 0 & \sin(\theta) \\ 0 & 1 & 0 \\ -\sin(\theta) & 0 & \cos(\theta) \end{bmatrix} \\
 L_{IB} &= [\Psi][\Theta][\Phi] = \begin{bmatrix} c(\psi) & -s(\psi) & 0 \\ s(\psi) & c(\psi) & 0 \\ 0 & 0 & 1 \end{bmatrix} \begin{bmatrix} c(\theta) & 0 & s(\theta) \\ 0 & 1 & 0 \\ -s(\theta) & 0 & c(\theta) \end{bmatrix} \begin{bmatrix} 1 & 0 & 0 \\ 0 & c(\phi) & -s(\phi) \\ 0 & s(\phi) & c(\phi) \end{bmatrix}
 \end{aligned} \tag{A.3}$$

Finally, body force components are obtained from:

$$\begin{aligned}
 R_{mf_B} &= [L_{BW}]R_{mf_W} \\
 R_{rf_B} &= [L_{BW}]R_{rf_W} \\
 R_{D_B} &= [\alpha_D][\Theta]R_{D_W} \\
 R_{R_B} &= [\alpha_R][\Theta]R_{R_W} \\
 R_{sail_B} &= [L_{BAWA}]R_{sail_{AWA}} \\
 R_{hull_B} &= [L_{IB}]'R_{hull_I}
 \end{aligned} \tag{A.4}$$

Moments about the CoG derive from the definition, by calculating the cross product between the vector distance between the centre of effort of the i -element and the force vector into body axes:

$$\begin{aligned}
 \vec{r}_i &= \begin{Bmatrix} x_g - x_i \\ y_g - y_i \\ z_g - z_i \end{Bmatrix} \\
 \vec{M}_i &= \vec{r}_i \times \vec{R}_{i_B}
 \end{aligned} \tag{A.5}$$

A.2 Inertia of the system

The inertia values could be evaluated in different ways, with analytic approach or from 3D CAD measurements. For the purpose of this thesis, reference values are given the work of Boegle [4] who applied a FE (finite element) approach to describe the inertia tensor of a moth with standard characteristic and geometry. In general, this represents an approximation for the current thesis work, since the geometry could change (and thus the inertia) as function of the **optimization tool** results. However, this error does not affect the model accuracy but can lead to a slight change in the P-I-D gains because a different boat reaction.

Focusing of the Boegle work, the inertia tensor of the boat is:

$$I_{boat} = \begin{bmatrix} I_{xx} & I_{xy} & I_{xz} \\ I_{xy} & I_{yy} & I_{yx} \\ I_{xz} & I_{yz} & I_{zz} \end{bmatrix} = \begin{bmatrix} 90.22 & 0 & -2.19 \\ 0 & 114.45 & 0 \\ -2.19 & 0 & 31.47 \end{bmatrix} [Kg \cdot m^2] \tag{A.6}$$

For the sailor contribution, he assumed the sailor body as composition of simple geometric bodies, then he calculated inertia tensor into sailor reference system and finally passed results into the body system. Results are provide in terms of gyradii matrix:

$$i_{sailor} = \begin{bmatrix} i_{xx} & i_{xy} & i_{xz} \\ i_{xy} & i_{yy} & i_{yx} \\ i_{xz} & i_{yz} & i_{zz} \end{bmatrix} = \begin{bmatrix} 0.36 & 0 & 0 \\ 0 & 0.3 & 0.24 \\ 0 & 0.24 & 0.35 \end{bmatrix} [m] \tag{A.7}$$

To convert the latter, into the tensor matrix is necessary to remember the gyradii definition:

$$i_{ij} = \text{sign}(I_{ij}) \sqrt{\frac{I_{ij}}{m}} \quad (\text{A.8})$$

Assuming a sailor mass of $75kg$, it gives:

$$I_{sailor} = \begin{bmatrix} I_{xx} & I_{xy} & I_{xz} \\ I_{xy} & I_{yy} & I_{yx} \\ I_{xz} & I_{yz} & I_{zz} \end{bmatrix} = \begin{bmatrix} 9.72 & 0 & 0 \\ 0 & 6.75 & 4.32 \\ 0 & 4.32 & 9.19 \end{bmatrix} [Kg \cdot m^2] \quad (\text{A.9})$$

By the end, the total inertia tensor of the system is:

$$I_{system} = I_{boat} + I_{sailor} = \begin{bmatrix} 99.94 & 0 & -2.19 \\ 0 & 121.2 & 4.32 \\ -2.19 & 4.32 & 40.66 \end{bmatrix} [Kg \cdot m^2] \quad (\text{A.10})$$

A.3 Control systems

The analysis of the control system mechanism involves numerous parameters and disciplines. In this thesis the model is simplified and aims to find a link between the flight height h (input) and the angle of flap α_{flap} (output). In the following the **Mach2** and **BugsCam** systems are distinguished due to different peculiarities concerning the functioning of the bow mechanism.

A.3.1 Mach2

The bow mechanism of **Mach2** is based on the circular movement of the control link, which is responsible of the horizontal translation Δx of the push rod. The mathematical model of the system consists of the following two equations:

- Equation of a line passing through the fixed pivot, joint with the lateral link and representing the connection between the fixed pivot and the control link:

$$f_{pivot} = \frac{x - x_p}{\tan(\epsilon)} + y_p \quad (\text{A.11})$$

- Equation of a circumference centred into the fixed pivot, representing the trajectory of the control link:

$$f_{controllink} = y_p - \sqrt{r^2 - (x - x_p)^2} \quad (\text{A.12})$$

Where:

- $\{x_p, y_p\} = \{2,2\}$ cm position of the fixed pivot;
- $r = 2$ cm length of the pivot;
- ϵ angle between the vertical direction and the direction of pivot. It is related to the α_{wand} through:

$$\alpha_{wand} = \epsilon - \max(\epsilon) \quad (A.13)$$

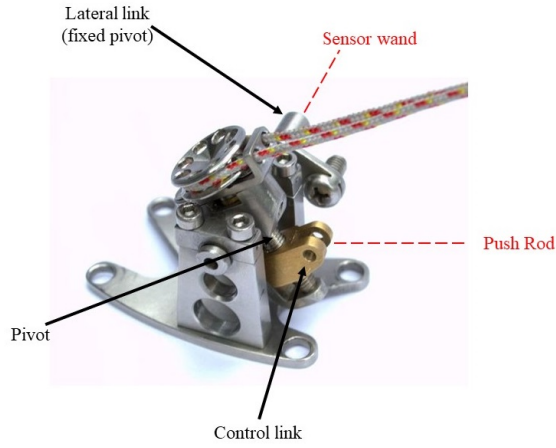


Figure A.1: Mach2: real system

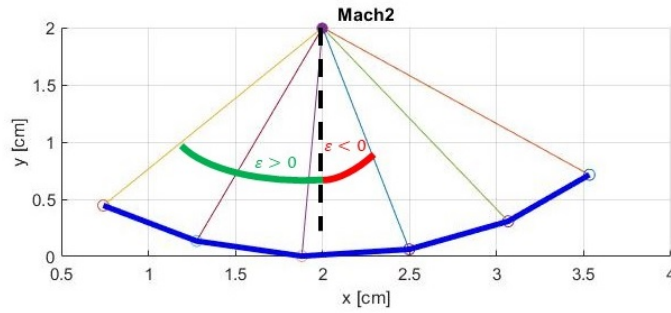


Figure A.2: Mach2: model variables

The problem's solution comes from imposing a value of ϵ and find the intersection between the two curves in order to obtain the correspondence value x . Iterating the process it is possible to correlate the horizontal translation of the push rod with the sensor wand rotation, thus representing the sensitivity of the system.

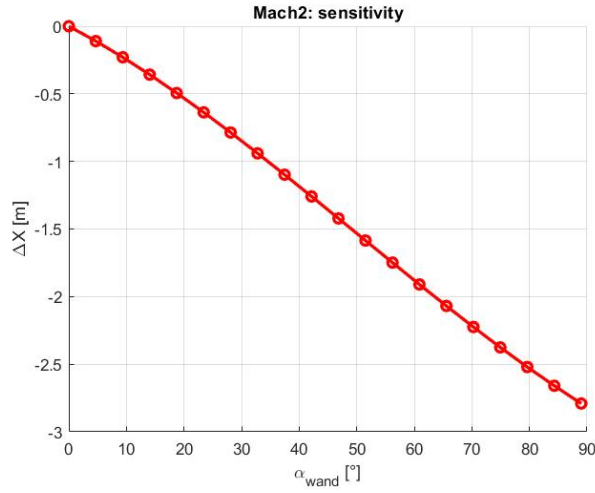


Figure A.3: Mach2: sensitivity

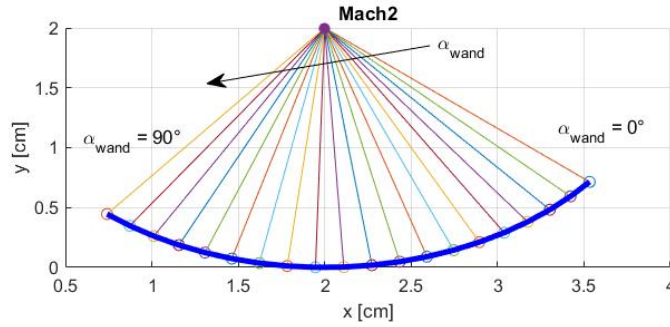


Figure A.4: Mach2: model

Moreover, considering a bell-crank ratio of 1 : 2, the vertical translation Δy is found and consequently the flap angle. This results in the total amount of flap deflection, and a further offset must be considered to impose the desired take off angle at 15° .

$$\alpha_{flap} = -\arcsin \frac{\Delta y}{c_{flap}} + 5^\circ \quad (\text{A.14})$$

The performance curve is thus obtained in figure A.5.

A.3.2 BugsCam

With reference to the article [10], the main idea on which the **BugsCam** system is founded, is to provide different sensitivities according to the flight condition and

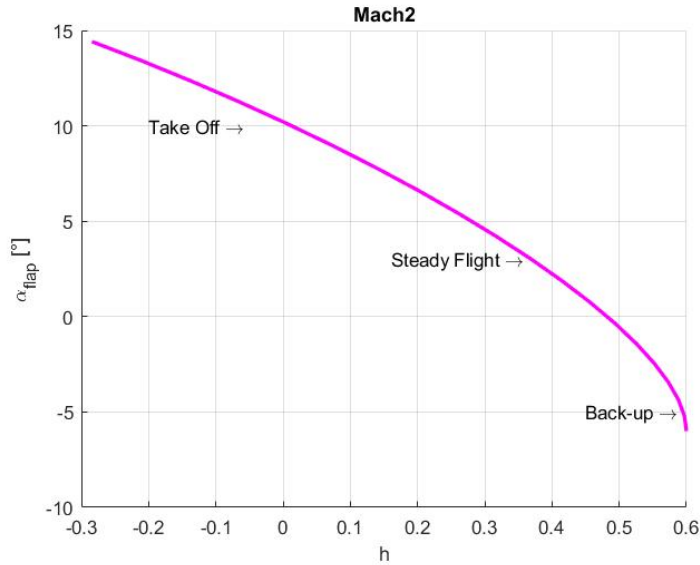


Figure A.5: Mach2: performance

avoid the implementation of gearing adjustment to reduce the sailor’s workload. The sensitivity is defined as the ratio between the vertical movement of the push rod and the angle swept by the wand:

$$sensitivity = \frac{\Delta y}{\alpha_{wand}} \quad (A.15)$$

It represents the main design parameter because the variables involved (e.g. flap angle and flight height) are directly connected each other from already presented equations.

The sensitivity is chosen to allow the craft to reach the steady state flight as quickly as possible, and to descend rapidly after the occurrence of a disturbance, through a “back-up” zone capable of immediately reducing lift, thus preventing the craft from jumping out of the water.

The typical regime flight condition corresponds to the **third zone**. It is characterized by a lower sensitivity in order to neglect effects of small disturbances and lead to a smoother flight condition. When severe perturbations, such as intense waves, occur, the more sensitive zones are activated. In particular, the “back-up” **zone 4** provides greater sensitivity for a range of 12° of wand angle. As far as take-off phase is concerned, the **first zone** shows a linear trend, gradually increasing in sensitivity. This means that at low rides the flap angle is almost constant and close to the maximum value. Finally, the **zone 2** can be seen as a “transition zone”, featured by the maximum sensitivity. Therefore, during the take-off, the flap

moves rapidly towards the steady state condition while, following a disturbance, it immediately provides more lift to return to the regime height.

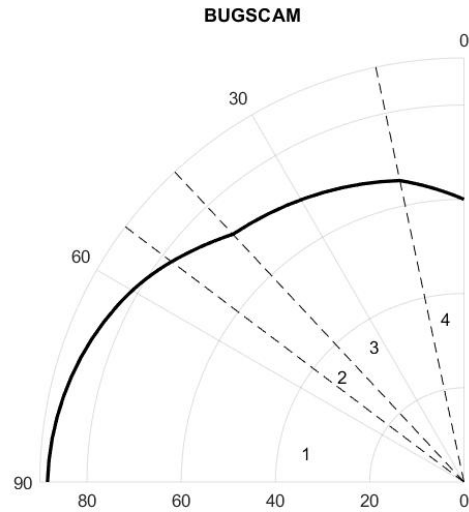


Figure A.6: BugsCam: curve

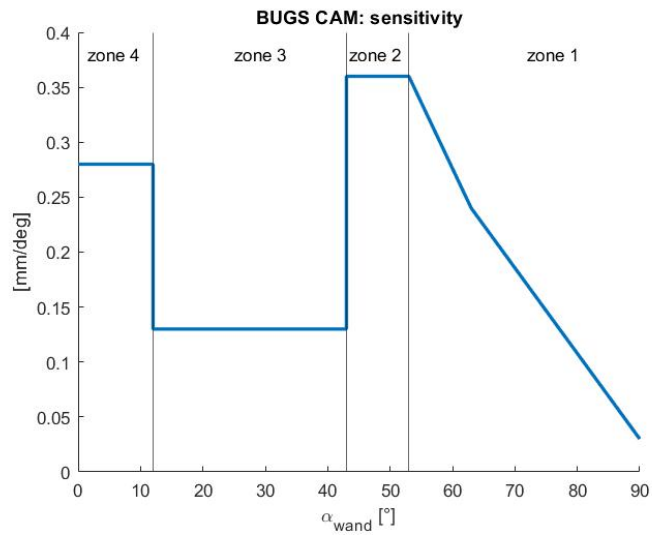


Figure A.7: BugsCam: sensitivity

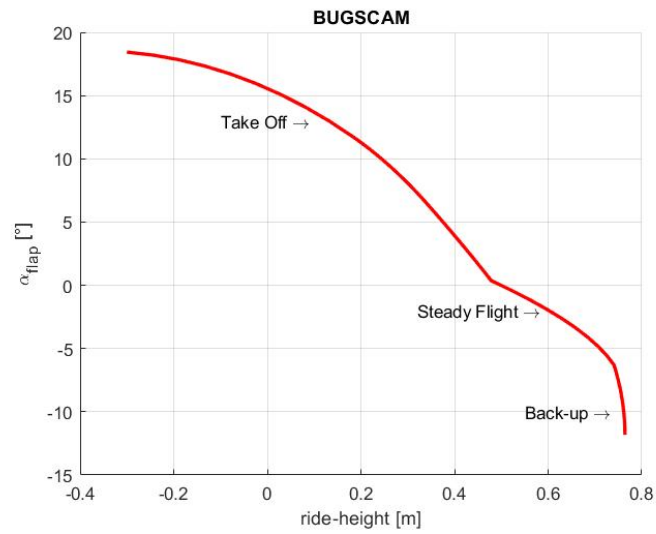


Figure A.8: BugsCam: performance

A.4 Fixed data

The fixed model data are resumed in the following table. Measurements are referenced from the bow and from the deck plane.

Boat and Sailor data		
Boat's mass	m_{boat}	30 Kg
Sailor's mass	m_{sailor}	75 Kg
Centre of Gravity	$\{x_g, y_g, z_g\}$	$\{2.1, 0, 0.755\} m$
Inertia	$\{I_{xx}, I_{yy}, I_{zz}\}$	$\{99.94, 121.2, 40.66\} kg \cdot m^2$
Cross-product inertia	$\{I_{xy}, I_{xz}, I_{yz}\}$	$\{0, -2.19, 4.32\} kg \cdot m^2$
Hull		
Platform surface	S_{hull}	0.8 m ²
Hull's height	h_{hull}	0.4 m
Hull's buoyancy line	$h_{buoyancy}$	0.2 m
Sail		
Centre of effort	$\{x_s, y_s, z_s\}$	$\{1.8, 0, 2.3\} m$
Surface	S_{sail}	8.2 m ²
Main foil		
Profile	NACA 63-412	/
Lift curve slope (2D)	a_{mf}	0.1165 $\frac{1}{\circ}$
Zero lift angle of attack	α_0	-3°
Setting angle	i_{mf}	4°
Flap derivative	τ	0.4
Oswold factor	e	0.85
Rudder foil		
Profile	NACA 63-412	/
Lift curve slope (2D)	a_{rf}	0.1165 $\frac{1}{\circ}$
Zero lift angle of attack	α_0	-3°
Setting angle	i_{rf}	0°
Oswold factor	e	0.85
Daggerboard		
Profile	NACA 0012	/
Lift curve slope (2D)	a_D	0.1 $\frac{1}{\circ}$
Water Length	L_D	0.95 m
Oswold factor	e	0.95
Rudder		
Profile	NACA 0012	/
Lift curve slope (2D)	a_R	0.1 $\frac{1}{\circ}$
Water Length	L_R	0.94 m
Oswold factor	e	0.95

Table A.1: fixed model data

Bibliography

- [1] DNV GL Maritime. *FS-Equilibrium User manual*. Potsdam, Germany, 2014 (cit. on p. 2).
- [2] Alec Bagué, Joris Degroote, Toon Demeester, and Evert Lataire. «Dynamic Stability Analysis of a Hydrofoiling Sailing Boat using CFD». In: *Journal of Sailing Technology* 6.01 (Mar. 2021), pp. 58–72. ISSN: 2475-370X. DOI: 10.5957/jst/2021.6.1.58. eprint: <https://onepetro.org/JST/article-pdf/6/01/58/2478473/sname-jst-2021-04.pdf>. URL: <https://doi.org/10.5957/jst/2021.6.1.58> (cit. on p. 2).
- [3] Rafael Tannenbergh. «Comparison of Hydrodynamic Models for the Velocity Prediction of Foiling Yachts». M. Eng. thesis. Southampton, United Kingdom: University of Southampton, 2020 (cit. on pp. 2, 6, 8, 18).
- [4] Christian Bögle. «Evaluation of the Performance of a Hydro-Foiled Moth by Stability and Force Balance Criteria». M. Eng. thesis. Berlin, Germany: Technische Universität Berlin, 2010 (cit. on pp. 2, 11, 12, 41, 67).
- [5] Fabio Eggert. «Flight Dynamics and Stability of a Hydrofoiling International Moth with a Dynamic Velocity Prediction Program (DVPP)». M. Eng. thesis. Berlin, Germany: Technische Universität Berlin, 2018 (cit. on pp. 2, 9, 44, 47).
- [6] International Sailing Federation. *INTERNATIONAL MOTH CLASS RULES*. Southampton, United Kingdom, May 2017 (cit. on p. 2).
- [7] Alan Block. *Bladerider Moth Sailboat*. 2007. URL: <https://www.sailingworld.com/sailboats/bladerider-moth-sailboat/> (cit. on p. 3).
- [8] *Points of sail*. URL: <https://www.pinterest.it/pin/227713324881756082/> (cit. on p. 6).
- [9] www.mach2boats.com. *Mach2 shop*. URL: <https://www.kasail.com/mach2/product> (cit. on p. 8).
- [10] Avalon Sail. *Latest update on the BUGS CAM*. Western Australia, 2018. URL: <https://avalonsails.com.au/blog/2018/3/14/latest-update-on-the-bugs-cam> (cit. on pp. 9, 70).

- [11] Airfoil Tools. *NACA 63-412 AIRFOIL*. URL: <http://airfoiltools.com/airfoil/details?airfoil=n63412-il> (cit. on p. 14).
- [12] Airfoil Tools. *NACA 0012 AIRFOIL*. URL: <http://airfoiltools.com/airfoil/details?airfoil=n0012-il> (cit. on p. 14).
- [13] Paul Kaplan, Pung N.Hu, and Stavros Tsakonas. «Methods for estimating the longitudinal and lateral dynamic stability of hydrofoil craft». In: *Stevens Institute of Technology E.T.T. Report No. 691*, (1958) (cit. on pp. 17, 22).
- [14] M. V. Cook. *Flight Dynamics Principles - A Linear Systems Approach to Aircraft Stability and Control*. Oxford: Butterworth-Heinemann, 2013. ISBN: 978-0-080-98242-7 (cit. on pp. 19–22, 41).
- [15] Y. Masuyama. «Performance of a hydrofoil sailing boat (2 nd report)». In: *journal of the Society of Naval Architects of Japan* (1982) (cit. on pp. 28, 55).
- [16] MathWorks. *Genetic Algorithm*. URL: <https://it.mathworks.com/discovery/genetic-algorithm.html> (cit. on p. 29).
- [17] MathWorks. *MultiStart*. URL: <https://it.mathworks.com/help/gads/multistart.html> (cit. on p. 29).
- [18] Abderrahmane Badis. «Subsonic Aircraft Wing Conceptual Design Synthesis and Analysis». In: *International Journal of Sciences: Basic and Applied Research (IJSBAR)* 35 (Aug. 2017), pp. 64–108 (cit. on p. 30).
- [19] Mario E. Salgado Graham C. Goodwin Stefan F. Graebe. *Classical PID Control*. Control System Design, Prentice Hall PTR (cit. on p. 44).
- [20] Heikki Hansen. «Enhanced Wind Tunnel Techniques and Aerodynamic Force Models for Yacht Sails». PhD Thesis. Auckland, New Zealand: The University of Auckland, 2006 (cit. on p. 48).
- [21] *4 key basic actions to master steering a rc sailboat*. URL: <https://dockstahavet.se/blog/basic-actions-to-master-steering> (cit. on p. 59).
- [22] *X-FOIL Subsonic Airfoil Development System*. URL: <https://web.mit.edu/drela/Public/web/xfoil/> (cit. on p. 64).
- [23] MathWorks. *Linear-Quadratic Regulator*. URL: <https://it.mathworks.com/help/control/ref/lqr.html> (cit. on p. 64).
- [24] MathWorks. *H-Infinity Synthesis*. URL: <https://it.mathworks.com/help/robust/controller-synthesis.html> (cit. on p. 64).